GEOMAGNETIC INDUCTION STUDIES IN EASTERN NEWFOUNDLAND

BADAL KANTI PAL

GEOMAGNETIC INDUCTION STUDIES IN EASTERN NEWFOUNDLAND

by

Badal Kanti Pal, M.Sc.

A Thesis submitted in partial fulfillment
of the requirements for the degree of
Master of Science

Department of Earth Sciences
Memorial University of Newfoundland

February 1983

St. John's Newfoundland

ABSTRACT

An electromagnetic induction study has been carried out in the period range 40 seconds to 1 second at eight stations in eastern Newfoundland. The results show that conductivity anomalies in the Gander-Avalon zone are mainly associated with geological boundaries and faults.

Because of the dominance of coast effect in the area, the signature of the inland induction anomaly in the observed data is separated from the superimposed coast effect by applying a difference arrow analysis technique. Difference arrows are obtained by taking a vector subtraction of the analogue model coast effect induction arrows from the observed induction arrows, based on assumption that the mutual inductance between the conducting ocean and any lithospheric conductor is small and can be neglected to a first order approximation. The most important feature apparent from this study is a zone of high conductivity under the Gander-Avalon boundary.

Two dimensional numerical modelling is used to test models that are compatible with existing geological and geophysical results. A fossil oceanic lithospheric slab remnant from past subduction associated with the closure of the proto-Atlantic ocean is modelled on 25 × 30 grid. Two models, an east-dipping subduction model and an obduction model are shown to be quantitatively consistent with the observations. On the basis of these observations,we are unable to

distinguish between these two models. The model of east-dipping subduction places the slab at a depth of 5 km and dipping eastward under the Gander Avalon boundary. The obduction model places the slab at the same depth as the previous model. However, it is extended laterally 28 km into the Avalon zone compared to 22 km as inferred from the previous model. A conductivity of 0.04 s/m which is the typical conductivity of hydrous minerals is determined as the conductivity of the slab.

ACKNOWLEDGEMENTS

I wish to sincerely thank my supervisor Dr. J.A. Wright for suggesting this research topic. I am indebted to him not only for his advice and guidance but also for the enthusiastic encouragement and kindness he has shown me throughout my research work. I would further wish to thank him for the use of previously developed computer programs.

I would like to thank Dr. H.G. Miller for many useful and stimulating discussions. I like to thank Mr. Dan Walker for assistance in the field trips and Mr. Tom Laidley for assistance in writing computer programs. Thanks must also go to friend Eugenio Madruga who has also assisted me in the field testing trips.

I am also grateful to the Department of Physics and Department of Earth Sciences for providing facilities for my research and also to the members of the department who have assisted me in innumerable ways.

I thank Mrs. Gerri Starkes for the difficult job of typing the manuscript and Mr. W. Howell for his drafting assistance.

I express my appreciation to Memorial University of Newfoundland for providing financial support in the form of a Graduate Fellowship and teaching assistantship; financial support from NSERC

grant A7505 to Dr. J.A. Wright is also acknowledged.

Finally, I wish to thank my wife, Manisha, for her patience and constant encouragement, particularly during the final months.

TABLE OF CONTENTS

LIST OF TABLES

LIST OF FIGURES

PAGE

PAGE

PAGE

CHAPTER 1

INTRODUCTION

1.1 Electromagnetic induction in the Earth

The study of electromagnetic induction in the Earth by natural time-varying magnetic fields has been revealing more and more information regarding the conductivity distribution of the Earth. Induction studies may be broadly classified into two groups. The first is global studies which deal with the electromagnetic induction in a radially symmetric Earth. A discussion of such global studies is given by Price (1973) and a review of the methods and results of global geomagnetic sounding is given by Bailey (1973). The second is regional studies in which the induced fields observed at a site are explained by induction in regional conductors. During the last decade, there has been increasing attention given to the second kind of investigation.

The varying magnetic fields observed at the surface of the Earth consists of two parts; a primary field produced by magnetospheric and ionspheric current flow and a secondary field induced in the upper layers of the Earth by the primary fields. In the absence of any underground inhomogeneities, the induced currents would follow the pattern of the external field. But this is rarely observed in practice and most of the stations are somewhat anomalous (Cochrane and Hyndman, 1970). Induced internal currents consisting of a normal and an anomalous part flow with a distribution determined by the conductivity structure

in the Earth. The normal part is interpreted in terms of regional effect and the anomalous part is interpreted in terms of the anomalous conductivity distribution.

The frequency of the inducing field is of interest because it determines the depth of penetration of the inducing field through the skin depth effect. High frequency variations in the inducing field induce strong eddy currents which according to Lenz's law, act to reduce the amplitude of the disturbing variations and do not penetrate deep into the Earth. On the other hand, low frequency variations penetrate deeper into the conductor. Thus the electromagnetic induction studies allow probing of the conductivity structure.

Reports of geomagnetic anomalies associated with lateral inhomogeneities in conductivity have appeared frequently in the literature. Schmucker (1970) has described three types of anomalies: 1) surface anomalies, which are due to superficial conductivity variations above the crystalline basement; 2) intermediate anomalies, which are connected with insulated conductors in the high resistivity zone of the Earth's crust and upper mantle; and 3) deep anomalies, which reflect conductivity imbalances in the upper mantle.

The anomaly due to abrupt change in conductivity between land and sea at the ocean-continent interface is included in the first type of anomaly of Schmucker. According to this anomaly, the vertical component of the geomagnetic variation field is greatly enhanced near coast-lines and correlates positively with the inland horizontal

component. This is the so called 'geomagnetic coast effect', first reported by Parkinson (1959) and also observed by many others (Everett and Hyndman, 1967; Schmucker, 1970; Cochrane and Wright, 1977; Rikitake, 1966). This effect is usually attributed to the effects of currents induced in the sea, but some results of theoretical studies state that currents induced in the ocean alone cannot explain this effect fully (Parkinson and Jones, 1979).

There are also other kinds of anomalies connected with the conductive structures in the crust of the Earth. Porath and Dziewonski (1971) reported anomalies associated with deep basins filled with sedimentary rocks. Dyck and Garland (1969) gave a concept of current concentration anomaly in a body of high conductivity which joins unknown regions in which induction occurs. Edwards *et al*. (1971) reported leakage from the deep ocean around British Isles. Law and Riddihough (1971) suggested anomalies associated with geological boundaries marking ancient plate margins. According to Gough (1973), 'in the crust current concentration anomalies are the rule rather than exceptions'.

1.2 Geomagnetic induction studies in Newfoundland

Very few geomagnetic variation studies have been done in Newfoundland. Hyndman and Cochrane (1971) analyse two stations (St. John's and Stephenville) and observe large coast effect at St.John's. Bailey *et al*. (1974) also analyse two stations (Deer Lake and St. John's) and report a similar type of coast effect at period 3870 sec. Systematic studies in Newfoundland are described by Cochrane and Wright (1977) and Wright and Cochrane (1980). The large coast effect observed in eastern

Newfoundland is explained by them as the consequence of current channeling about the eastward projecting corner of Newfoundland. Furthermore, Wright and Cochrane (1980) identify an induction anomaly associated with the line of closure of the proto Atlantic ocean.

In an attempt to find the behaviour of induced magnetic fields in complex coastal regions of Newfoundland, Hebert *et al.* (1983) conducted an analogue model study of Newfoundland. Their results show a large enhancement in the magnetic field over the straits and deflection of induced currents around the capes. Dosso *et al.* (1980) also report similar enhancement in the magnetic field for a traverse T_2 which passes through the eastern portion of Newfoundland.

1.3 Geological setting

Although Newfoundland can be divided into three tectonic-stratigraphic zones, i.e. western platform, central mobile belt and avalon platform (Williams, 1964), the subdivision of Newfoundland into four structural-stratigraphic zones by Williams (1979) introduces a degree of regionality that appears useful for interpretation of the general geophysical trends. From west to east these are denoted as the Humber, Dunnage, Gander and Avalon zones.

The Humber zone in the western part of Newfoundland records the development and destruction of an Atlantic type continental margin, i.e. the ancient continental margin of Eastern North America. This zone consists of a crystalline basement, formed during the Grenville

orogeny and overlain by mainly sedimentary rocks.

The Dunnage zone is recognized by mainly mafic volcanic rocks with associated cherts, slates, greywackes and minor limestone (Williams and King, 1977). As this zone is dominated by mafic volcanic rocks and associated marine sediments locally overlying the ophiolite suite, Williams (1979) interpretes the Dunnage zone as the vestiges of a proto-Atlantic ocean, Iapetus.

The rocks of the Dunnage zone are much less deformed in comparison to nearby parts of the Humber and Gander zones. The eastern margin of this zone is the Dunnage Melange which occupies a wide belt consisting of a variety of volcanic and sedimentary blocks. The Dunnage Melange and related rocks are interpreted as the site of an oceanic trench and subduction (Kay, 1976; McKerrow and Cocks, 1977, 1978).

The eastern margin of the Dunnage zone includes a linear, northeast trending belt of discontinuous mafic-ultramafic rocks and these are overlain unconformably by conglomerates at the base of a sequence of Caradocian (450-440 Ma) black shales and slates which are a part of the Davidsville group (Williams and King, 1977).

The ultramafics of the Gander river ultramafic belt are interpreted as being slices of oceanic crustal material similar to that of the Dunnage zone to the west. Pajari and Currie (1978) have considered this line as a zone of imbricate, obducted ophiolite slices thrust over the Gander group. The Gander zone consists mainly of

pre-middle Ordovician rocks (Gander group) that are in most places poly-deformed and metamorphosed, thus resembling clastic rocks at the east margin of the Humber zone on the opposite side of the Iapetus. The thick polydeformed sequence of the zone is interpreted as a prism of sediment built up parallel to an existing shore line, the eastern margin of Iapetus (Kennedy, 1976). The eastern boundary of the Gander zone is drawn at the Dover fault which separates metamorphic rocks to the west from late Precambrian sedimentary and volcanic rocks of the Avalon zone to the east. The Dover fault is 300m-500m wide mylonite zone formed by the mylonitization of rocks of both the Gander and Avalon zones (Blackwood and Kennedy, 1975).

The Avalon zone consists mainly of thick sequences of late Precambrian volcanic and sedimentary rocks locally overlain by Paleozoic sediments with body and trace fossils characteristic of the Atlantic realm. The Avalon zone and Dunnage zone are separated from each other by the Gander zone and the Avalon zone did not directly face the Iapetus ocean. Furthermore, the Avalon zone was a stable platform during the Cambrian period when the generation and destruction of Iapetus was most active. Geochemical analysis in this area shows that there is a 'definite increase in the average potassium content from west to east across the Gander zone' (Strong *et al.*, 1974). The plutons of the eastern Avalon zone do not show this trend. This is interpreted by Strong *et al.* (1974) as evidence for an eastward dipping descending lithospheric slab (under the Avalon zone) related to the closure of the Iapetus ocean.

1.4 Geophysical evidence

There is some geophysical evidence which favours subduction to the south-east beneath the Avalon zone. Sheridan and Drake (1968) from seismic refraction studies at sea adjacent to Newfoundland observe that a crustal layer with a seismic velocity of 7-7.5 km/sec beneath the central and eastern portions of Newfoundland follows a regular pattern dipping to the southeast with respect to the pre-Carboniferous surface. It is close to the surface near the south-eastern edge of the Grenville orogen, beneath which it does not extend. At that edge of the Humber zone lies the ophiolite suites that are the remnants of the Paleozoic ocean (Williams, 1975). Williams (1975) suggested that western Newfoundland ophiolites were obducted over westward-dipping subduction zone. Gabbros and ultramafics within ophiolites have compressional velocities 6.8-7.4 km/sec and 8.4 km/sec respectively (Salisbury and Christensen, 1978) which are comparable to those within the major layers of ocean crust (Christensen and Salisbury, 1975). Such velocities are not found below the Grenville and can be traced downdip to the southeast, beneath the Avalon peninsula. This south eastward dip of the oceanic crustal layer and its presence beneath the Avalon zone is interpreted by Haworth *et al*. (1978) as an indication of subduction beneath the Avalon zone. Stewart (1978) observes that the p-p arrivals in Europe from Central American earthquakes are missing for a reflection zone adjacent to the western margin of the Avalon zone. He also suggests that this 'shadow zone' could be due to asymetry in the teleseismic reflection path which might be caused by the residual effect of a dipping subduction zone.

In gravity surveys in the central and northeastern Newfoundland (Miller and Deutsch, 1973, 1978; Weaver, 1967), the gravity signature across the boundary of Iapetus is distinct. The gravity data show a rapid transition from large positive anomalies associated with oceanic crustal material to near zero or negative anomalies over Gander zone. However, Miller and Weir (1982) observe an anomaly belt having signs of denser, more magnetic body beneath the granites of the Gander group east of the Gander River Ultramafic Belt. They interpret this anomaly as obducted ophiolitic materials emplaced in the continental rise prism represented by the Gander group sediments.

Wright and Cochrane (1980) and Cochrane and Wright (1977) from geomagnetic studies across Newfoundland identified a zone of high conductivity with the line of closure of the proto-Atlantic ocean. Wright and Cochrane (1980) correlate this anomaly with a remnant descending lithospheric slab embedded in the crust and upper mantle. However, their analysis do not say anything about the true direction of dip.

1.5 Conductivity values expected

According to geological and geophysical evidence (Strong *et al.*, 1974; Haworth *et al.*, 1978;Haworth and Keen, 1979), eastern Newfoundland is associated with geological boundaries marking ancient plate margins and paleozoic subduction. Most continental type rocks are quite resistive at the temperatures expected in the crust and upper mantle (Parkhomenko, 1967). In metamorphic areas, conductivity anomalies may be associated with

extensive mineralization resulting in massive sulphide or graphite bodies (Rooney, 1976) and in shear zones it may be due to the presence of conductive graphites (Wright and Cochrane, 1980). In eastern Newfoundland, there is no evidence of wide spread graphite zones or other surficial good conductors. However, crystalline rocks rich in hydrated minerals and containing appreciable free water may become very conductive at moderate temperature ($<700^{o}C$) (Greenhouse and Bailey, 1981). This includes amphibolites and serpentinites which are constituents of the oceanic crust (Christensen and Salisbury, 1975). The problem now is to explain the presence of either free water or water of hydration in such old crystalline rocks. Greenhouse and Bailey (1981) showed that a combined mechanism of Hyndman and Hyndman (1968) and Feldman (1976) may solve this problem. The dehydrated lower crust (Hyndman and Hyndman mechanism) may be rehydrated by the slow infusion of juvenile water from the under-thrust oceanic crust over zones of subduction (Feldman mechanism).

So, supposing that subduction has occurred at the ancient plate margin during paleozoic time, the observed conductivity anomaly could be associated with the hydrated minerals of the oceanic crust.

1.6 Outline of thesis

In this thesis, electromagnetic induction studies in the period range 1 sec to 40 sec are carried out for eight stations in eastern Newfoundland. Chapter 2, on the theory of electromagnetic induction in the Earth, first describes Maxwell's equations for two

dimensional structures and applied them to find the solution for the one-dimensional case. Different methods of solutions of two-dimensional models are reviewed and numerical solution via network synthesis technique is discussed.

Chapter 3 describes the instrumentation and data acquisition in the field. It also describes the method employed for calibrating the induction coils.

Chapter 4 deals with the method of data reduction. It includes the theoretical background for estimating the transfer function and processing of the raw data.

In Chapter 5, the estimated transfer functions are interpreted by plotting the induction and difference arrows. Difference transfer functions are then modelled numerically using a two-dimensional Earth-model.

Chapter 6 contains the summary and conclusions.

CHAPTER 2

THEORETICAL FORMULATIONS

The Geomagnetic depth sounding (GDS) method of investigating the electrical conductivity distribution in the Earth is based on the study of the natural transient magnetic field variations at the surface of the Earth. The basic theory relates to solving the problem of electromagnetic induction in the Earth by the natural time varying magnetic fields which propagate from the magnetosphere and are incident on the Earth's surface. In this chapter, theory for one and two dimensional models is considered.

2.1 Theory of Electromagnetic Induction

To formulate the problem of electromagnetic induction in the Earth, consider the Earth to be a uniform half space of conductivity σ, permittivity ε and permeability μ. A plane electromagnetic wave characterized by the magnetic vector $\vec{H}$, the electric vector $\vec{E}$ and the propagation vector $\vec{K}$ is incident on the Earth at any angle relative to the surface. In any source free medium, Maxwell's equations in the rationalized M.K.S. units are

$$\text{curl } \vec{H} = \vec{J} + \frac{\partial \vec{D}}{\partial t} \qquad 2\text{-}1$$

$$\text{curl } \vec{E} = - \frac{\partial \vec{B}}{\partial t} \qquad 2\text{-}2$$

$$\text{div } \vec{B} = 0 \qquad 2\text{-}3$$

$$\text{div } \vec{D} = 0 \qquad 2\text{-}4$$

with

$$\vec{J} = \sigma\vec{E} \qquad 2\text{-}5$$

$$\vec{D} = \varepsilon\vec{E} \qquad 2\text{-}6$$

$$\vec{B} = \mu\vec{H} \qquad 2\text{-}7$$

$$\mu = \mu_r\mu_o \qquad 2\text{-}8$$

where μ_r is the relative permeability of the medium.

For harmonic time variation of the form $e^{i\omega t}$, the above equations become

$$\text{curl } \vec{H} = (\sigma + i\omega\varepsilon)\ \vec{E} \qquad 2\text{-}9$$

$$\text{curl } \vec{E} = -i\omega\mu\vec{H} \qquad 2\text{-}10$$

$$\text{div } \vec{H} = 0 \qquad 2\text{-}11$$

$$\text{div } \vec{E} = 0 \qquad 2\text{-}12$$

which may be combined to give the vector Helmholtz equation

$$\nabla^2\vec{H} + k^2\vec{H} = 0 \qquad 2\text{-}13$$

where a rectangular Cartesian coordinate system is assumed and

$$k^2 = \omega\mu(i\sigma - \omega\varepsilon) \qquad 2\text{-}14$$

A similar equation exists for $\vec{E}$ field.

In the Earth, the magnetic permeability μ remains very close to that of free space and can be taken equal to $\mu_o = 4\pi \times 10^{-7}$ Henry/meter. For the range of parameters normally encountered in low frequency GDS surveys, displacement currents in the Earth can be neglected.

i.e. $\omega\varepsilon \ll \sigma$

or $$k^2 = i\omega\mu_o\sigma \qquad 2\text{-}15$$

The Helmholtz equation reduces to a diffusion equation. The solution field does not freely propagate, but decays exponentially with depth depending upon the frequency and conductivity of the medium. A useful measure of the effective depth of penetration is the 'skin depth δ' which is the depth at which the field amplitude is reduced to e^{-1} of its surface value. Thus the skin depth is given by

$$\delta = \left(\frac{2}{\mu_o \omega \sigma}\right)^{1/2} \quad , \qquad 2\text{-}16$$

At the interface between the two media, the boundary conditions are

$$E_{t1} = E_{t2}$$

$$H_{t1} = H_{t2}$$

$$\frac{1}{\rho_1} E_{n1} = \frac{1}{\rho_2} E_{n2}$$

$$\mu_1 H_{n1} = \mu_2 H_{n2}$$

where t and n represent tangential and normal field components respectively and the resistivity $\rho = 1/\sigma$.

First consider the case of a two-dimensional Earth model where the conductivity is a function of two space coordinates, say x and z. The coordinate axes are aligned such that positive z is down, x is north oriented and y east. The propagation vector $\vec{K}$ may be decomposed into two components K_{xz} and K_{yz} in the xz and yz planes respectively. Along the y-axis, the conductivity is constant. The one-dimensional model can be treated as the special case of the two-dimensional model.

Suppose, the direction of propagation is in the xz plane. Then the plane wave can be separated into two independent modes:

1) E-polarization and,

2) H-polarization

using the component representation for Maxwell's equations and remembering that y-derivatives of all the components vanish, one obtains the following:

E-polarization:

$$E_x = E_z = 0 = H_y$$

$$E_y = E_y(x,z)$$

From equation (2-9)

$$\frac{\partial H_x}{\partial z} - \frac{\partial H_z}{\partial x} = \frac{E_y}{\rho} \qquad 2\text{-}17$$

From equation (2-10)

$$-\frac{\partial E_y}{\partial z} = -i\omega H_x \mu_o \qquad 2\text{-}18$$

$$\frac{\partial E_y}{\partial x} = i\omega H_z \mu_o \qquad 2\text{-}19$$

H-polarization:

$$H_x = H_z = 0 = E_y$$

$$H_y = H_y(x,z)$$

From equation (2-9)

$$-\frac{\partial H_y}{\partial z} = \frac{1}{\rho} E_x \qquad 2\text{-}20$$

$$\frac{\partial H_y}{\partial x} = \frac{1}{\rho} E_z \qquad 2\text{-}21$$

From equation (2-10)

$$\frac{\partial E_x}{\partial z} - \frac{\partial E_z}{\partial x} = -i\omega\mu_o H_y \qquad 2\text{-}22$$

Thus for E-polarization, the complete field is specified by the solution of the equations

$$\frac{\partial^2 E_y}{\partial x^2} + \frac{\partial^2 E_y}{\partial z^2} - k^2 E_y = 0 \qquad 2\text{-}23$$

$$H_x = \frac{1}{i\omega\mu_o} \frac{\partial E_y}{\partial z} \qquad 2\text{-}24$$

$$H_z = \frac{1}{i\omega\mu_o} \frac{\partial E_y}{\partial x} \qquad 2\text{-}25$$

and for H-polarization, the equations are

$$\frac{\partial^2 H_y}{\partial x^2} + \frac{\partial^2 H_y}{\partial z^2} - k^2 H_y = 0 \qquad 2\text{-}26$$

$$E_x = -\rho \frac{\partial H_y}{\partial z} \qquad 2\text{-}27$$

$$E_z = \rho \frac{\partial H_y}{\partial x} \qquad 2\text{-}28$$

Thus, the solution of the electromagnetic induction problem is now reduced to finding the solutions of the scalar equations (2-23) to (2-28) subject to the appropriate boundary conditions.

2.2 Solution for a one-dimensional Earth model

i) Homogeneous half-space:

This is the simplest case of the one-dimensional problem in which the conductivity σ constant. The variation of the field components along x-direction vanishes reducing equations (2-23) to (2-28) to the simpler form given by

E-polarization

$$\frac{\partial^2 E_y}{\partial z^2} - k^2 E_y = 0 \qquad 2\text{-}29$$

$$H_x = \frac{1}{i\omega\mu_o} \frac{\partial E_y}{\partial z} \qquad 2\text{-}30$$

$$H_z = 0 \qquad 2\text{-}31$$

H-polarization

$$\frac{\partial^2 H_y}{\partial z^2} - k^2 H_y = 0 \qquad 2\text{-}32$$

$$E_x = -\rho \frac{\partial H_y}{\partial z} \qquad 2\text{-}33$$

$$E_z = 0 \qquad 2\text{-}34$$

The solutions of the above differential equations can be given in general by

$$E_y = Ae^{-kz} + Be^{kz} \qquad 2\text{-}35$$

$$H_x = \frac{-k}{i\omega\mu_o} (Ae^{-kz} - Be^{kz}) \qquad 2\text{-}36$$

$$H_y = A'e^{-kz} + B'e^{kz} \qquad 2\text{-}37$$

$$E_x = k\rho(A'e^{-kz} - B'e^{kz}) \qquad 2\text{-}38$$

Equations (2-35) to (2-38) represent physically damped waves propagating in the positive and negative z- directions. For a physically acceptable solution, the fields cannot increase indefinitely with increasing depth so that B and B' must be zero. The wave impedance or 'Cagniard impedance' of the homogeneous ground for two polarizations is written as

$$-\frac{E_y}{H_x} = \frac{E_x}{H_y} = \frac{i\omega\mu_o}{k}$$

ii) N-layered Isotropic half-space

In this model, the Earth is represented by a set of horizontal layers each having a different conductivity. Equations (2-29) to (2-34) are still valid for any layer. The solution in the m th layer is given by

$$E_{ym} = A_m e^{-k_m z} + B_m e^{k_m z}$$

$$H_{ym} = -\frac{k_m}{i\omega\mu_o} (A_m e^{-k_m z} - B_m e^{k_m z}) \; ; z_{m-1} < z < z_m$$

Applying the boundary conditions at the interface $z = 0$, $z=z_1, .., z=z_{m-1}$ and remembering that only outgoing waves ($B_m = 0$) are permissible in the lowest layer (which is semi infinite), one can find the unknown coefficients in terms of the known coefficient A_o. The solution is (Wait, 1962)

$$\frac{B_o}{A_o} = \frac{P_o - Q_1}{P_o + Q_1}$$

where

$$P_m = \left(\frac{\sigma_m}{i\omega\mu_o}\right)^{1/2}$$

and

$$Q_m = P_m \frac{Q_{m+1} + P_m \tanh(k_m h_m)}{P_m + Q_{m+1} \tanh(k_m h_m)}$$

An identical expression also exists for H-polarization case.

In this model also, there is no z- component of the magnetic field. So, for the homogeneous one dimensional model, the anomalous z magnetic field is zero and GDS method is not suitable for such structures.

2.3 Two-dimensional Earth model

Solutions for two dimensional Earth models are obtained by solving differential equations (2-23) to (2-28) for appropriate boundary conditions. Exact solutions of these equations are very difficult to obtain. However, there are some analytical solutions for relatively simple models. For example d'Erceville and Kunetz (1962) and Weaver (1963) have solved vertical fault problem; Rankin (1962) has solved dyke and Geyer (1972) dipping bed.

Another method of solving two-dimensional problems is the method of approximate solutions. Approximate solutions are obtained using numerical methods such as, the finite difference technique, the finite element technique and the integral equation method. Much work has been done on the induction effect in the ocean utilising these techniques. In general, three types of geometrical shape of the ocean-continent boundary are considered. In the first type, boundaries within the conductor separate regions of different but uniform conductivity; the second type considers the conductivity as a continuously variable function of the spatial coordinates. The third type of the ocean continent boundary is the ocean overlying a sloping sea floor. This is known as the inclined fault problem. The theoretical approach to this type of problem has been done by Neves (1957) and Dosso (1966). Tątrallyay and Jones (1974) have solved the problem of an asymetrical sloping contact ocean model for E-polarization using a perturbation technique. Jones and Price (1970) solve a similar problem for vertical edge. Lines *et al*. (1973) investigated the case

of E-polarization for three realistic models of ocean, crust and continental boundary. Bailey (1977), Nicholl and Weaver (1977), Brewitt-Taylor (1975, 1976) have attempted a two-dimensional model consisting of perfectly conducting half-plane representing an ocean-edge lying on and in electrical contact with the surface of a uniformly conducting half space representing the Earth's crust and solved for H-polarization. Fischer *et al.* (1978) have extended the calculations for E-polarization case.

There is yet another approximate method, namely, the network synthesis technique. In this method of solution, the equations (2.17) to (2.22), for E and H polarizations, are solved by a finite difference technique using the transmission line analogy. According to this analogy, the two-dimensional conductivity surface is represented by an equivalent transmission surface with a finite number of grid points. These points or nodes are linked by inductive or resistive impedances (Z) to adjacent points and by capacitative or resistive admittances (Y) to the ground depending on the mode of polarization. The transmission surface equations are discretized to fit the mesh (consisting of unit cells). The solution for voltage at each node is obtained by writing Kirchoff's current law for each node. For a mesh of $m \times n$ points with appropriate boundary conditions, the equation of current continuity produces $m \times n$ linear equations. The equivalence of voltage (V) with field parameters is as follows:

E-polarization

$$E_y \overset{\leftarrow}{\rightarrow} V$$

$$H_x = -\frac{\partial V}{\partial z} \cdot \frac{1}{i\mu_o\omega}$$

$$H_z = \frac{\partial V}{\partial x} \cdot \frac{1}{i\mu_o\omega}$$

H-polarization

$$H_y \overset{\leftarrow}{\rightarrow} V$$

$$E_x = -\frac{\partial V}{\partial z}\,\rho$$

$$E_z = \frac{\partial V}{\partial x}\,\rho$$

$$\sigma \overset{\leftarrow}{\rightarrow} Z$$

$$i\mu\omega \overset{\leftarrow}{\rightarrow} Y$$

This method of network synthesis has been used extensively by Swift (1967), Wright (1969) and Cochrane (1972) and is the technique utilized in this work.

CHAPTER 3

INSTRUMENTATION AND DATA ACQUISITION

Good quality data critically depends on good instrumentation. This chapter deals with the instrumentation used in the field for detection and recording the variations in the components of the geomagnetic field. A short discussion on the data acquisition and calibration of the measuring instruments is also included in this chapter.

3.1 Instrumentation

The system used in obtaining the data presented herein is shown in the block diagram of figure 3.1. The magnetic field components are measured by means of three induction coil magnetometers. Each coil is comprised of ∿200,000 turns of #40 wire wound on ferrite core of 30 mm diameter and 1300 mm in length. The coils are encased in weather proof plastic housings which act to attenuate thermal perturbations.

For measurements in the field, the coils are installed as shown in figure 3.2. The signals from each coil are first passed through a low-noise pre-amplifier having a gain of 50. Then the signals are carried by a long cable to the recording truck which is parked about 200 m from the coils. In the truck, the pre-amplified signals are passed through three identical Butterworth filters/amplifiers (.001 HZ to 10 HZ pass) one for each channel to avoid aliasing. Figures 3.3, 3.4 and 3.5 show the circuit diagram, amplitude and phase response of the filter/amplifiers.

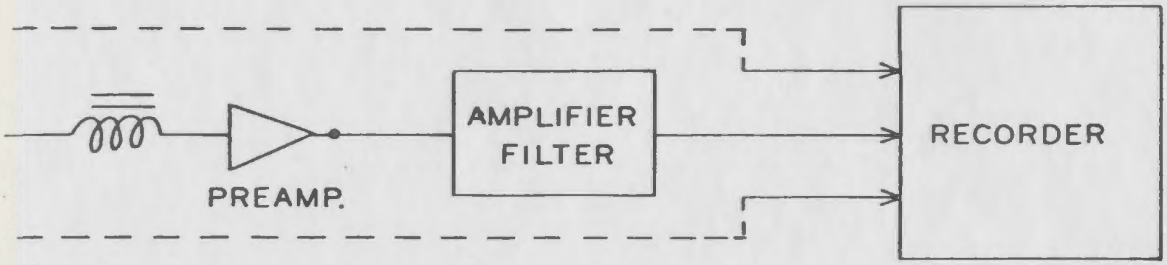

Fig. 3.1 Block diagram of recording system.

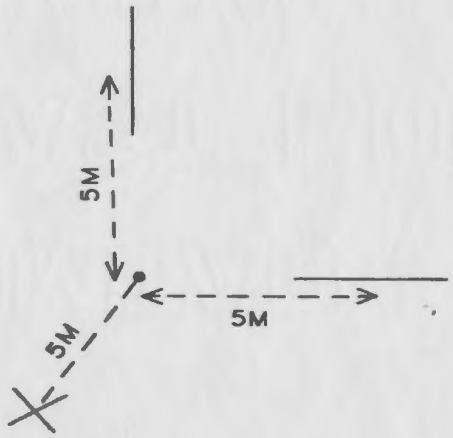

Fig. 3.2 Setup of induction coils in the field.

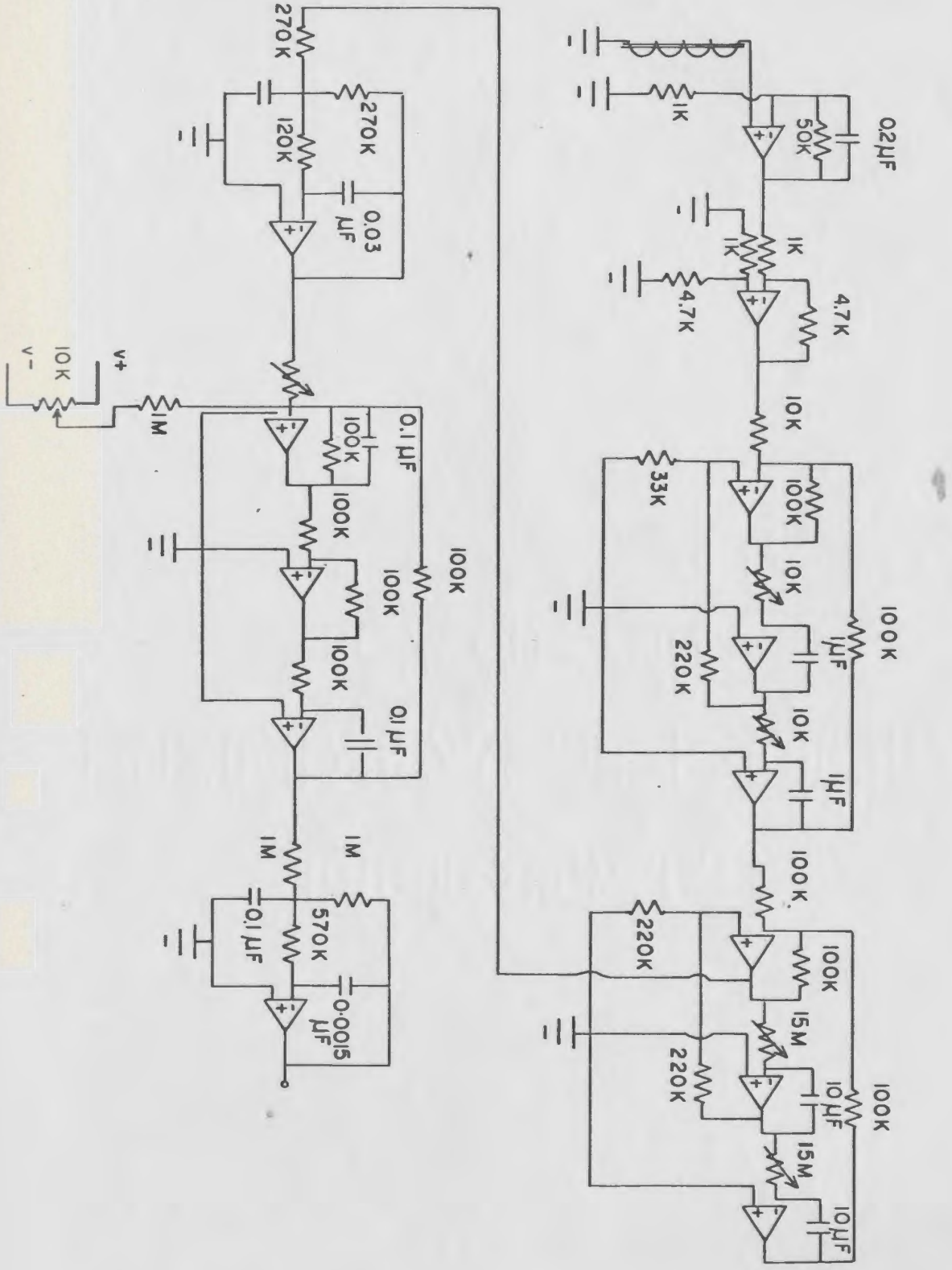

Fig. 3.3 Schematic circuit diagram of amplifers/filters.

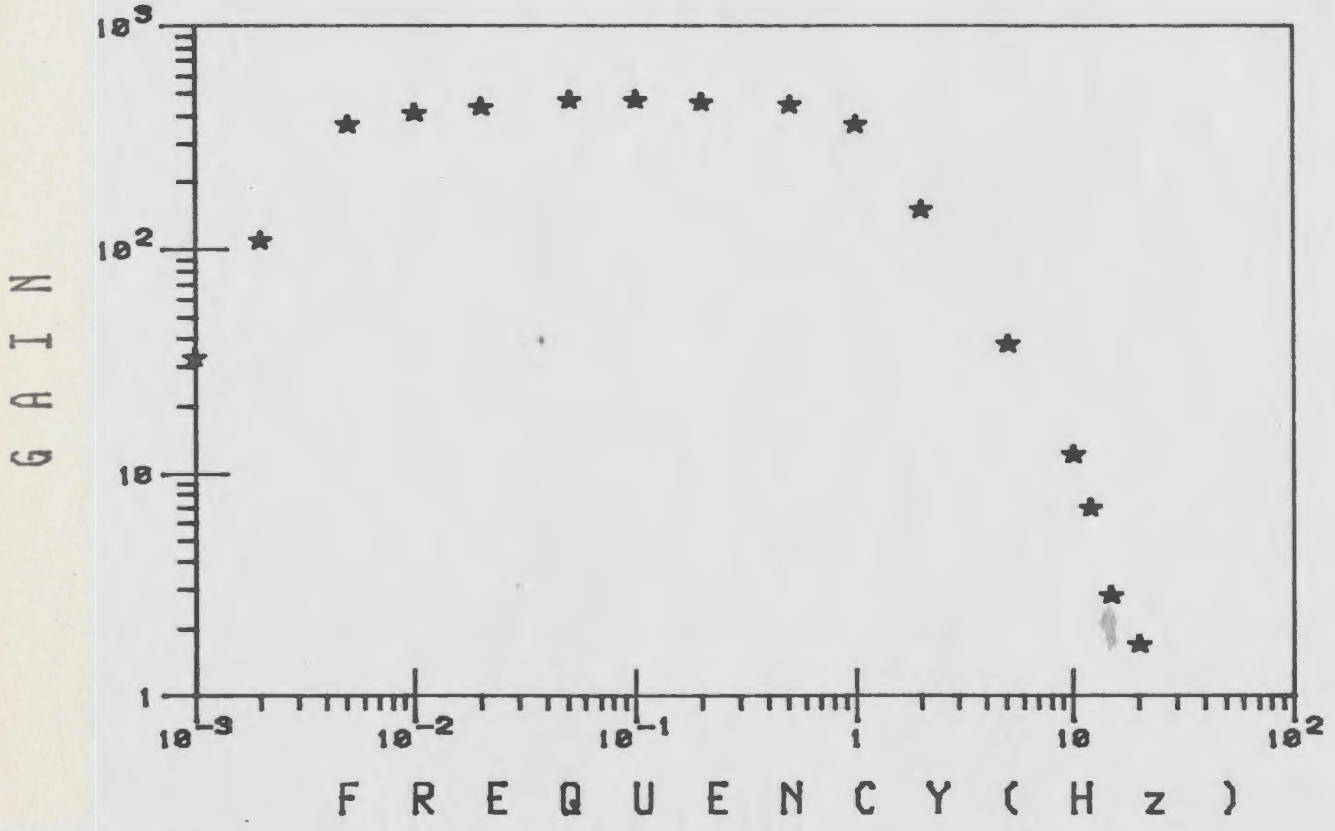

Fig. 3.4 Gain response of amplifers/filters.

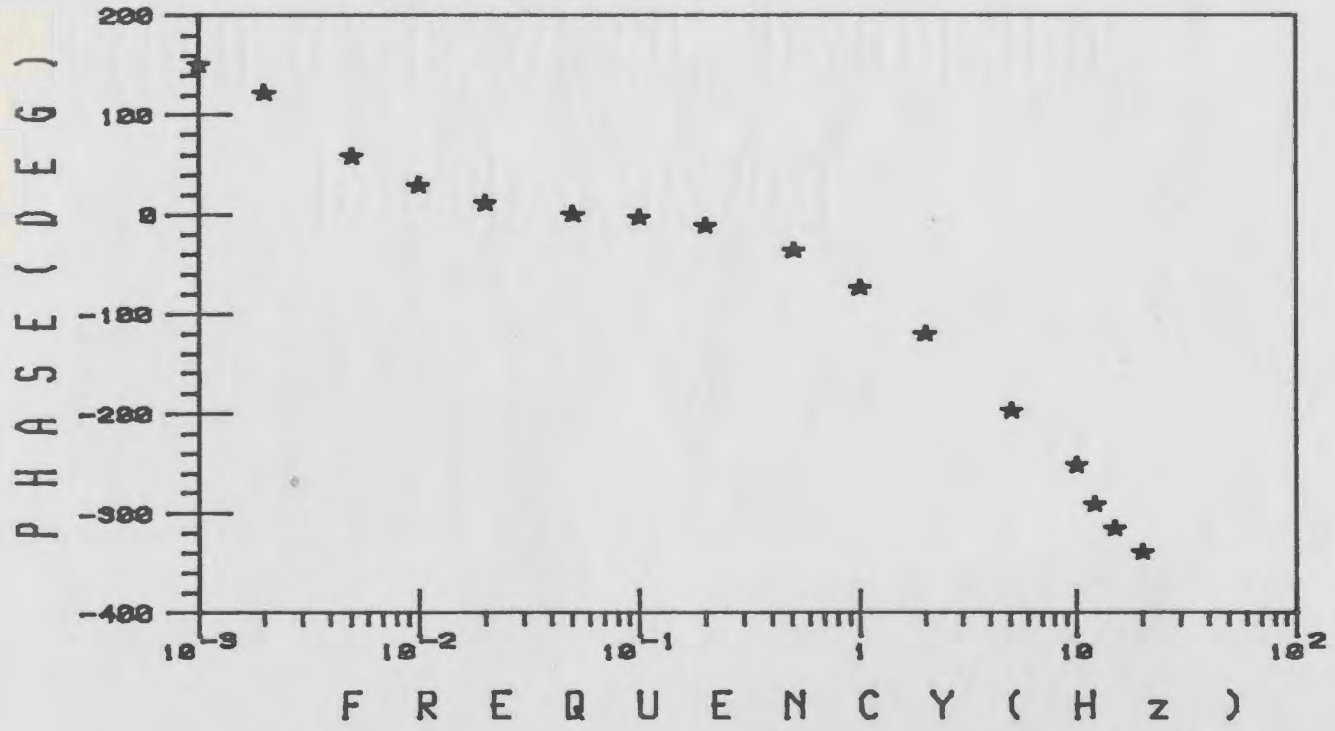

Fig. 3.5 Phase response of amplifiers/filters.

The recording instrument is a battery powered microcorder (Teledyne MCR 600). This is an analogue to digital recorder with data being recorded on cassette tapes. The signals from the filter/amplifier are multiplexed into one channel of the microcorder. The multiplexer was designed for six inputs; three for magnetic components, two for tellurics and one constant voltage for calibration and channel identification. The signals are recorded on the tape according to the following format

channel	components
0	H
1	D
2	Z
3	E_x
4	E_y
5	constant voltage

3.2 Data acquisition

The data were acquired during the summer of 1982. Figure 3.6 and table 3.1 show the locations of the observation sites. After setting up the instruments in the field and prior to starting recording, the connections are again checked and the signals are viewed on an oscilloscope. When a signal with good activity is observed, the recording is commenced and continues until a full cassette has been

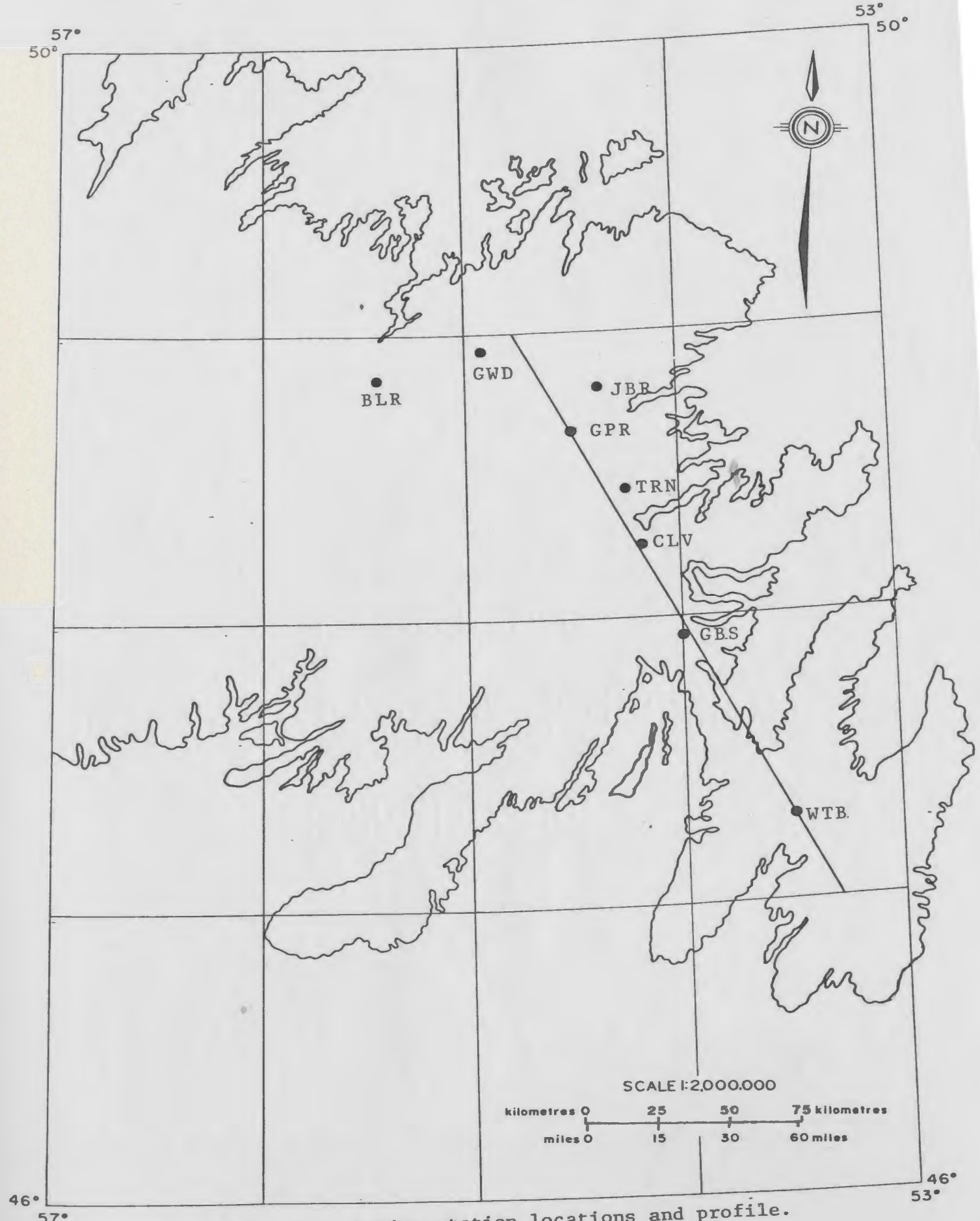

Fig. 3.6 Map showing station locations and profile.

recorded. At a digitizing rate of 150 HZ, one tape holds twenty five minutes of data. Two such tapes are collected for each station.

TABLE 3.1

LIST OF STATIONS AND LOCATIONS

STATION	ABBREVIATION	N. LAT.	E. LONG.
WHITBOURNE	WTB	47°17'	53°29'
GOOBIES	GBS	47°57'	53°59'
CLARENVILLE	CLV	48°14'	54°12'
TERRA NOVA	TRN	48°29'	54°13'
GAMBO POND ROAD	GPR	48°40'	54°31'
JOE'S BROOK ROAD	JBR	48°51'	54°30'
GLENWOOD	GWD	48°58'	54°57'
BORNEY LAKE ROAD	BLR	48°56'	55°29'

The tapes recorded in the field are then played back onto the computer in the laboratory using the microcorder play back unit (Teledyne MCP 650). As the data are in ASCII Code, they are converted into real data, demultiplexed and stored in files using a computer program. Demultiplexed data are then plotted and selected portions with good activity are noted for processing. All stations except one (JBR) gave good data allowing processing of 4K and 8K long data

seta. Table 3.2 shows the number of 4K and 8K long data sets employed for processing at each station and utilised in the interpretation.

TABLE 3.2

NO. OF 4K AND 8K DATA SETS
FOR EACH STATION

STATION	NO. OF DATA SETS	
	4K	8K
WTB	14	8
GBS	9	6
CLV	12	8
TRN	6	3
GPR	12	8
JBR	3	2
GWD	4	7
BLR	12	8

3.3 Calibration of the Induction coils

Calibration of the measuring instruments is accomplished by employing a calibrated Helmholtz coil and is performed for each induction coil separately with the same form of set up as used in the field (except for the recording instrument). Each induction coil is placed at a known distance from the centre of the axis of the Helmholtz coil such that the axes of the Helmholtz and induction coils are parallel to each other. The output from the filter/amplifier is now connected to an oscilloscope. The Helmholtz coil is excited by a current source from

a signal generator and the field produced by the coil at a distance r is calculated according to the relation (Telford *et al.*, 1976)

$$B \simeq \frac{2\mu_o INa^2}{4r^3}$$

where in M.K.S. units

N = No. of turns on each Helmholtz coil

I = current in Amperes

a = radius of the Helmholtz coil

μ_o = permeability of the free space

r = distance from the centre of the Helmholtz coil

The above approximate relation introduces an error in the calculated field which is less than 3% for $r \geq 7a$. The field induces an E.M.F. in the induction coil which is measured from the peak-to-peak reading on the oscilloscope. The distance of the Helmholtz coil from the induction coil is adjusted in order to get a maximum response of the induction coil signal without distortion. The measurements are repeated for eight frequencies and for each frequency the amplitude response of the induction coil in volts/nT is calculated. The process is repeated for three coils and the response is plotted against frequency on a semi-logarithmic scale. The responses at periods greater than 10 sec are based on the relative response of the D and Z coils with respect to the H-coil. This procedure is valid as this portion of the response is far away from the self resonances of the coils (see fig. 3.7). The calibration factors are applied to the spectral estimates to give the spectra in magnetic field values (nT). The algorithm for transforming the data into spectral form is discussed in Chapter 4.

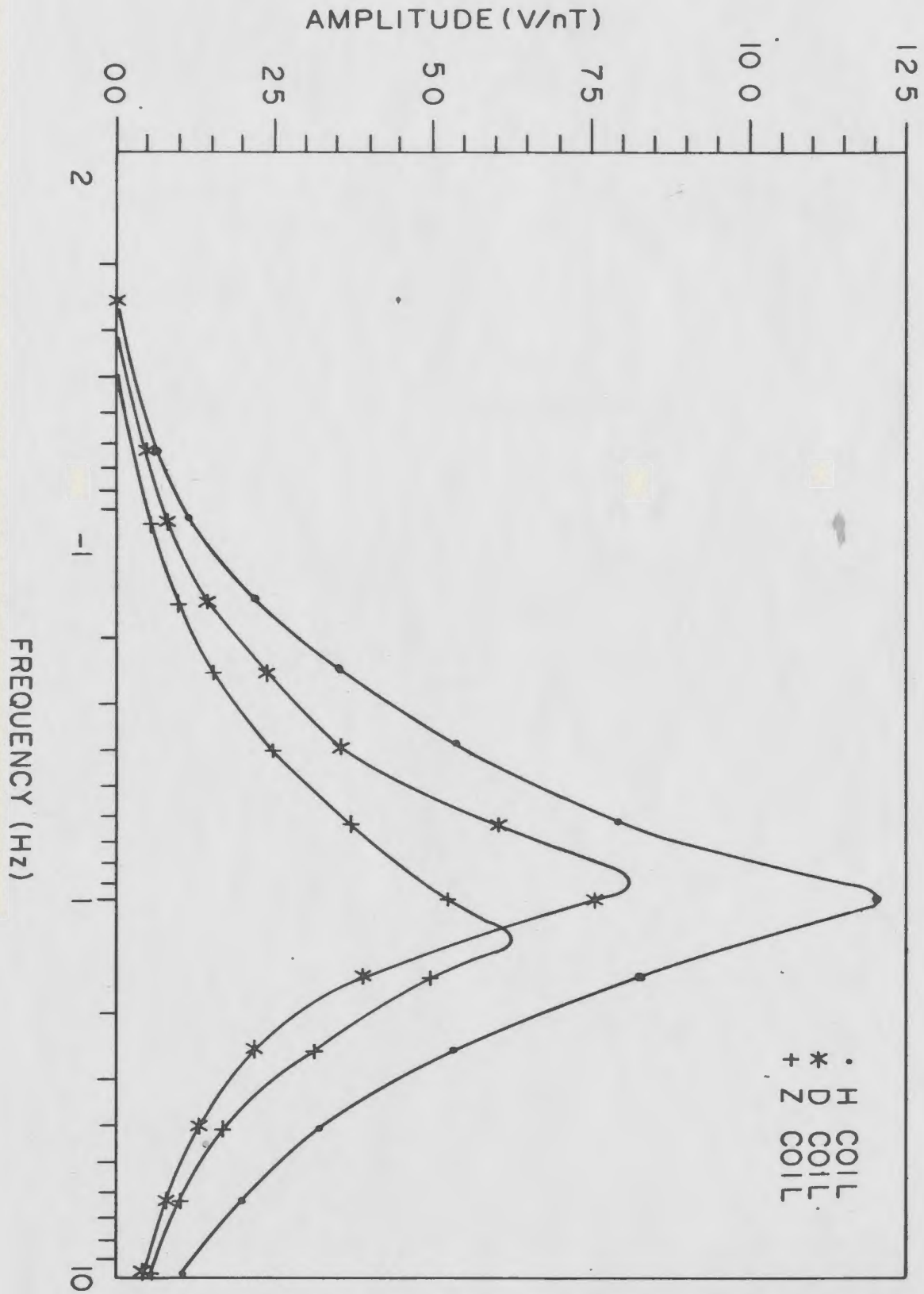

Fig. 3.7 Amplitude response of induction coils.

CHAPTER 4

DATA REDUCTION

The geomagnetic data recorded in the field are subjected to refined analysis in order to extract reliable values of the parameters for direct comparison with the model derived values. One such parameter of particular interest in this study is the vertical transfer function. Since the interpretation of the geomagnetic data is usually carried out in the frequency domain, the raw data are processed using spectral analysis techniques.

This chapter deals with the theoretical formulation of transfer functions and processing of raw data for estimating the spectra and transfer functions.

4.1 Transfer function

A ground based geomagnetic measurement provides a measure of the magnetic field vector $\vec{B}(t)$ with components H(t), D(t) and Z(t). H(t) is oriented north-south, D(t) is east-west and Z(t) is vertically downward in the northern hemisphere. The measurement of these field components at a site is a sum total of the response of the localized small scale and large regional structures. The inducing magnetic field may be visualized as the field which would exist at an observation site if the Earth there were a horizontally-stratified, isotropic medium. This is called the normal field (H_N, D_N, Z_N). Deviation from this ideal condition gives rise to anomalous fields (H_a, D_a, Z_a). Parkinson (1959) and Weise (1962) observed that the vertical magnetic field could be correlated with the horizontal

magnetic field components. This relation between the vertical and horizontal components of geomagnetic variations at a particular station implies that the vector changes of the geomagnetic field tend to lie in a particular plane, called by Parkinson the 'preferred plane' which is tangential to the conductivity surface at depth. 'Induction arrows' or 'induction vectors' are used to visualize graphically on a map the orientation and qualitative intensity of the underground conductivity structure.

There are different conventions and methodologies used to derive the induction arrows. Gregori and Lanzerotti (1980) have reviewed the different graphical methods and the relationship between the arrows produced by each method. One such method is the transfer function technique developed by Schmucker (1964, 1970), Everett and Hyndman (1967), Cochrane and Hyndman (1970), Banks (1973) and Frazer (1974). This method utilises the statistical treatment for the detection and separation of anomalous internal fields from the observed variation data.

Because of the linearity of Maxwell's equations, the anomalous and normal geomagnetic field components are linearly related in the frequency domain by a matrix of transfer functions

$$\begin{pmatrix} H_a \\ D_a \\ Z_a \end{pmatrix} = \begin{pmatrix} h_H & h_D & h_Z \\ d_H & d_D & d_Z \\ z_H & z_D & z_Z \end{pmatrix} \begin{pmatrix} H_N \\ D_N \\ Z_N \end{pmatrix} + \begin{pmatrix} \varepsilon_H \\ \varepsilon_D \\ \varepsilon_Z \end{pmatrix} \qquad 4.1$$

The complex coefficients of the 3 × 3 array are functions of frequency and position and are called transfer functions. The last vector on the right hand side of equation (4.1) represents small residuals due to second order effects and becomes a minimum when the normal and anomalous parts of the field are completely separated. The residual then is a representation of the noise in the spectra.

Assuming ε_i close to zero, equation (4.1) may be written as

$$\begin{aligned} H_a &= {}^{h}_{H}H_N + {}^{h}_{D}D_N + {}^{h}_{Z}Z_N \\ D_a &= {}^{d}_{H}H_N + {}^{d}_{D}D_N + {}^{d}_{Z}Z_N \qquad 4.2 \\ Z_a &= {}^{z}_{H}H_N + {}^{z}_{D}D_N + {}^{z}_{Z}Z_N \end{aligned}$$

solutions of equations (4.2) require the determination of H_a, D_a, Z_a and H_N, D_N, Z_N from the observed data H, D, Z. If this can be done, the transfer functions can be estimated by calculating suitable cross-spectra. In practice, most stations are somewhat anomalous (Cochrane and Hyndman, 1970) and it is very hard to get a normal station for determining H_N, D_N and Z_N. Everett and Hyndman (1967) and Schmucker (1970) advanced methods for calculating the vertical transfer functions z_H and z_D. Multiplying each of the terms in the 3rd scalar equation in (4.2) by H^*_N, D^*_N and Z^*_N one gets

$$\begin{pmatrix} Z_a H^*_N \\ Z_a D^*_N \\ Z_a Z^*_N \end{pmatrix} = \begin{pmatrix} H_N H^*_N & D_N H^*_N & Z_N H^*_N \\ H_N D^*_N & D_N D^*_N & Z_N D^*_N \\ H_N Z^*_N & D_N Z^*_N & Z_N Z^*_N \end{pmatrix} \begin{pmatrix} z_H \\ z_D \\ z_Z \end{pmatrix} \qquad 4.3$$

In the mid-latitudes, the normal vertical component Z_N is very small (about 1/3 of the horizontal component) and assumed uncorrelated with the normal horizontal components. Therefore, setting cross-spectra with Z_N to zero, one obtains solutions for z_H and z_D as

$$z_H = \frac{(Z_a H^*_N)(D_N D^*_N) - (Z_a D^*_N)(D_N H^*_N)}{(H_N H^*_N)(D_N D^*_N) - (D_N H^*_N)(H_N D^*_N)} \qquad 4.4$$

$$z_D = \frac{(Z_a D^*_N)(H_N H^*_N) - (Z_a H^*_N)(H_N D^*_N)}{(H_N H^*_N)(D_N D^*_N) - (D_N H^*_N)(H_N D^*_N)} \qquad 4.5$$

In practice, however, one uses the single station analysis due to the difficulty in selecting a normal station. Hence, the field components H, D and Z rather than the H_N, D_N and Z_N are used in equations (4.4) and (4.5). The transfer functions arising from the horizontal components cannot be calculated by this method and will not be discussed in this thesis. Schmucker (1970) represented the transfer functions as a set of arrows. The real parts of z_H and z_D are combined to give an in phase induction arrow and the imaginary parts to give the quadrature induction arrow.

Induction arrows thus defined lie in the preferred plane but point away from zones of enhanced conductivity. The direction of the arrow is then reversed for consistency with the direction of the Parkinson vectors. Some investigators change the sign of the in phase arrow only (Schmucker, 1970; Cochrane and Hyndman, 1970, 1974) while others change the sign of the imaginary part as well (Gough *et al.*, 1973 ;

Frazer, 1974). Lilley and Arora (1982) argued that depending on the convention of time dependence used at the time of data processing, the direction of the quadrature arrow has to be reversed to conform with Parkinson's convention. They demonstrate that for the time dependence of $e^{-i\omega t}$, a quadrature arrow unreversed points toward a simple near surface channelling. On the other hand, for the time dependence of $e^{+i\omega t}$, the sign of the quadrature arrow must be reversed to point toward the near surface conductor. Since the data processing in this analysis utilises the later convention of time dependence, the direction of both in phase and quadrature arrows are reversed. Thus

$$\vec{A}_R = - \mathrm{Re}(z_H)\vec{i} - \mathrm{Re}(z_D)\vec{J}$$

$$\vec{A}_I = - \mathrm{Im}(z_H)\vec{i} - \mathrm{Im}(z_D)\vec{J}$$

The in phase arrow $\vec{A}_R$ will be much larger than the quadrature arrow $\vec{A}_I$ when large and deeper conductive bodies are involved. The quadrature arrow will be large when near surface layers are concerned for long period variations.

4.2 Data processing

The main purpose of data processing is to estimate reliable values of the transfer functions from the field data. There are a number of techniques for transforming the time series into spectral information e.g. Fourier harmonic analysis, Fourier transient analysis and power spectral analysis (see reviews Sims and Bostick, 1969; Hermance, 1973). The most popular and widely used technique among them is the power spectral analysis. According to this technique, the digitized

field components are Fast Fourier transformed (FFT) using the algorithm of Cooley and Tukey (1965). Then one calculates the auto-power and cross-power for each harmonic and finally, the power spectra are averaged over bands of frequencies to get the desired amount of smoothing.

The power spectral technique is based on the assumption that the digitized time series is quasi-stationary with zero mean. If the mean is not zero, the power spectrum will have a large estimate at d.c. which contaminates at other frequencies. This leakage of d.c. power is reduced by removing the mean of the data set.

The time series may have a slowly varying linear trend about which it may be oscillating. This may be due to drifting of measuring instruments or due to an actual underlying linear trend in the data over a long record length. Bendat and Piersol (1966) show that the presence of a linear trend causes large distortion of the spectral estimates, particularly at the low frequencies. This effect is reduced by subtracting the least squares line from each data set.

Power spectral estimates are most reliable when the power is distributed evenly over all frequencies. In most geomagnetic time series, it is observed that the power decreases significantly with increasing frequency. As emphasized by Hinich (1967), this will lead to leakage of low frequency energy through side lobes of the filter used during computation. To avoid such spectral distortion, the data

are passed through a filter which compensates or pre-emphasizes the frequencies with lower amplitudes. This process of bringing the resultant spectrum close to that of white noise is called prewhitening. A three point moving average filter is chosen for pre-whitening the data.

After the window has been applied, and the spectrum obtained, an inverse filter is applied to compensate for the pre-whitening. This is called 'post colouring' which restores the originally suppressed power levels for all frequencies. This compensation is effected by dividing the power spectrum by the square of the amplitude response of the pre-whitening filter.

Only a finite section of the continuous signal is digitized and used for spectral analysis. Truncation of a time series introduces distortion into the coefficients of the Fourier transform. Bath (1974) has shown that the truncation of a time series leads to biased spectral estimates. It is a convolution of the true spectrum and a box-car function $W(\omega) = \frac{\sin \omega T/2}{\omega T/2}$ which represents a certain smoothing of the true spectrum. The degree of smoothing depends on the window length T such that the shorter T is, the stronger is the smoothing effect. In addition to this, the window $W(\omega)$ introduces side-lobes which lead to undesirable effects. The side-lobes of the data window die out slowly and the negative side-lobes lead to spectral leakage (Bath, 1974).

This leakage of power from side-lobes into the central lobe may be kept close to minimum by applying a data window. A very popular

window is the cosine tapered rectangular window suggested by Tukey (1967) which is applied to 10% of each end of raw time series.

In the case of a time series of N points, the digital representation of the Fourier transform is

$$X_K(\omega) = \sum_{n=0}^{N-1} X_n \, \mathrm{EXP.}\left[\frac{-i2\pi K}{N\Delta t}\right] \Delta t.n$$

$$= \sum_{n=0}^{N-1} X_n \, \mathrm{EXP.}\left[\frac{-i2\pi Kn}{N}\right]$$

where $\Delta t = \frac{1}{2f_N}$ is the digitizing interval and K is an integer

$K = 0, 1, 2, \ldots N-1$.

The Fourier coefficients are given corresponding to frequencies

$$\omega_K = \frac{2\pi K}{N\Delta t}$$

The data sets are Fast Fourier transformed by employing the method of simultaneous computation of two Fourier transforms (Kanasewich, 1975). The cross and auto-power spectra for two time series X_n and Y_n are

$$P_{XY}(\omega) = X_K(\omega) \; Y^*_K(\omega)$$

$$P_{XX}(\omega) = X_K(\omega) \; X^*_K(\omega)$$

$$P_{YY}(\omega) = Y_K(\omega) \; Y^*_K(\omega)$$

where asterisks denote the complex conjugates. These give raw, unsmoothed cross and auto-power estimates.

The power spectral estimates so obtained display erratic behaviour and the variance of the estimates does not decrease as the length of the time series is increased. Even, if the record length

is made longer and longer, one may get a greater frequency resolution, but the statistical reliability does not increase. The variance of the estimate may be reduced by band averaging over N neighbouring frequencies. The variance then is proportional to $N^{-1/2}$ (Jones, 1965). Since the transfer function and frequency are plotted on semilog scales, a band smoothing with bands whose centre frequencies are equispaced on a logarithmic scale is followed. If n bands are desired in each frequency decade, the ratio of centre frequencies of adjacent bands is

$$\log \frac{f_{i+1}}{f_i} = \frac{1}{n}$$

Band width, in terms of the number of points of the transforms must also increase with frequency for consistent smoothing on a log-frequency scale. This means that different smoothed estimates are composed of averages of different number of raw estimates i.e. the variance is a function of f.

Each set of data at a station are processed using a Fortran programme according to the following sequence of operations:

1. From each component of the time series, the least squares best fit line and the mean are subtracted.

2. The data series are then prewhitened using a three point moving average filter with a prewhitening factor of 0.99.

3. Prewhitened data are then tapered using a Tukey cosine bell as discussed before in section 4.2.

4. A fast Fourier transform of the data is carried out employing a technique of simultaneous computation of two Fourier transforms. The Fourier transforms are used to calculate auto and cross-power spectra.

5. The auto and cross-power spectra are smoothed using a logarithmic band averaging technique.

6. Smoothed spectra are restored to their original power level by dividing the spectra by the square of the amplitude response of the prewhitening filter. The spectral data are stored in a computer file.

7. Calibration factors are applied to the smoothed spectra.

8. Transfer function estimates and coherency analysis are carried out for each event.

9. The amplitude and direction of in phase and quadrature arrows at each frequency are averaged over all the events analysed at the station to give the final estimate at the frequency.

10. The amplitude and direction of the arrows are plotted against period on a semi-logarithmic scale. Error bars of plus and minus one standard deviation are included on the plots to show

the scatter.

These results are presented and interpreted in the following chapter. The plots of the amplitudes and directions of the real (in phase) and imaginary (quadrature) arrows (averaged over all data) are presented in appendix A.

CHAPTER 5

INTERPRETATION

In this chapter, the field observations are interpreted on the basis of the previous geophysical and geochemical evidence (see sections 1.3 and 1.4). A qualitative description of the behaviour of the induction arrows is obtained by plotting the induction arrows corresponding to periods of 40 sec, 10 sec, 4 sec and 1 sec. The difference arrow analysis technique is followed to separate the signature of the inland anomaly in the experimental data from the superimposed coast effect. The resulting transfer functions are used as constraints to model the electrical conductivity structure under the Gander and Avalon zone.

5.1 Qualitative interpretation

The area of study in the northeastern part of Newfoundland covers the Avalon, Gander and a small portion of the Dunnage zone. This overlaps in part with that considered by Miller and Weir (1982). A general discussion on the geology of the zonal subdivisions of Newfoundland is given in section 1.3. Figure 5.1 shows the local geology in the area of study. Locally in the study area, the Dunnage zone is represented by the mafic-ultramafic rocks of the Gander River Ultramafic Belt overlain to the west by the shales and slates typical of the Dunnage zone. One station BLR is located on this structure. The eastern edge of this group is marked by the Gander River ultramafic belt and station GWD is situated on this. The Gander zone in the study area is represented by the Gander group of rocks and plutons intruding the Gander group where the stations GPR and JBR lie.

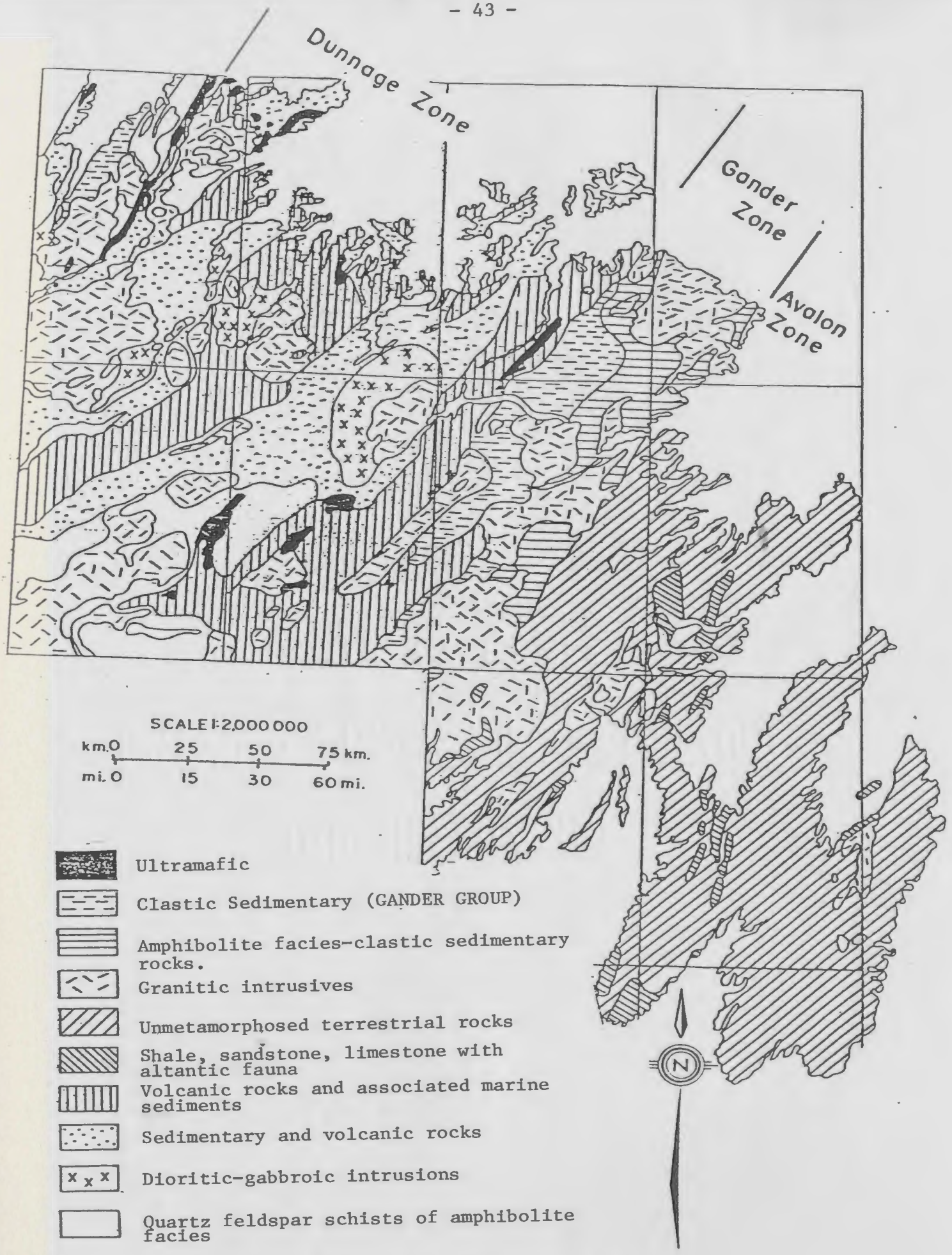

Fig. 5.1 Local geology of the area of study.

On the southeast of JBR lies the Dover fault which is the boundary between the Gander and the Avalon zones. This fault continues southwestward to Terra Nova Lake (Blackwood 1976). Station TRN is located close to this lake in the Avalon zone. Further southeast of TRN, there are three other smaller faults trending southwest in the Precambrian rocks of Avalon zone. Station CLV is situated near Terrenceville fault. The other two stations GBS and WTB are located in the Precambrian sedimentary and volcanic rocks of the Avalon zone.

The Bouguer gravity anomaly and magnetic anomaly along the profile (fig. 3.6) are shown in the figure 5.2. Part of the modelled gravity data are projected from Weir's (1971) profile along the Trans Canada Highway and others are taken from the gravity map series 53 and 55 of Dominion Observatories Branch. The source of the magnetic anomaly data is the geophysical series (aeromagnetic), Geological Survey of Canada. West of the Gander zone is a region of high positive anomalies associated with the oceanic crustal material of the Iapetus ocean (Miller 1977). In the Gander zone, the gravity anomaly is negative and the transition from the positive to negative anomalies coincides with the eastern edge of the ultramafic belt. Weaver (1967) explained the negative anomalies in the Gander zone as the effect of granites emplaced in the normal crustal sequence. East of the Gander River ultramafic belt, the gravity again rises in the centre of the granitic plutons. Miller and Weir (1982) interpret this anomaly in terms of a few models of which their preferred one is an ophiolitic slice emplaced in the continental rise prism represented by the Gander

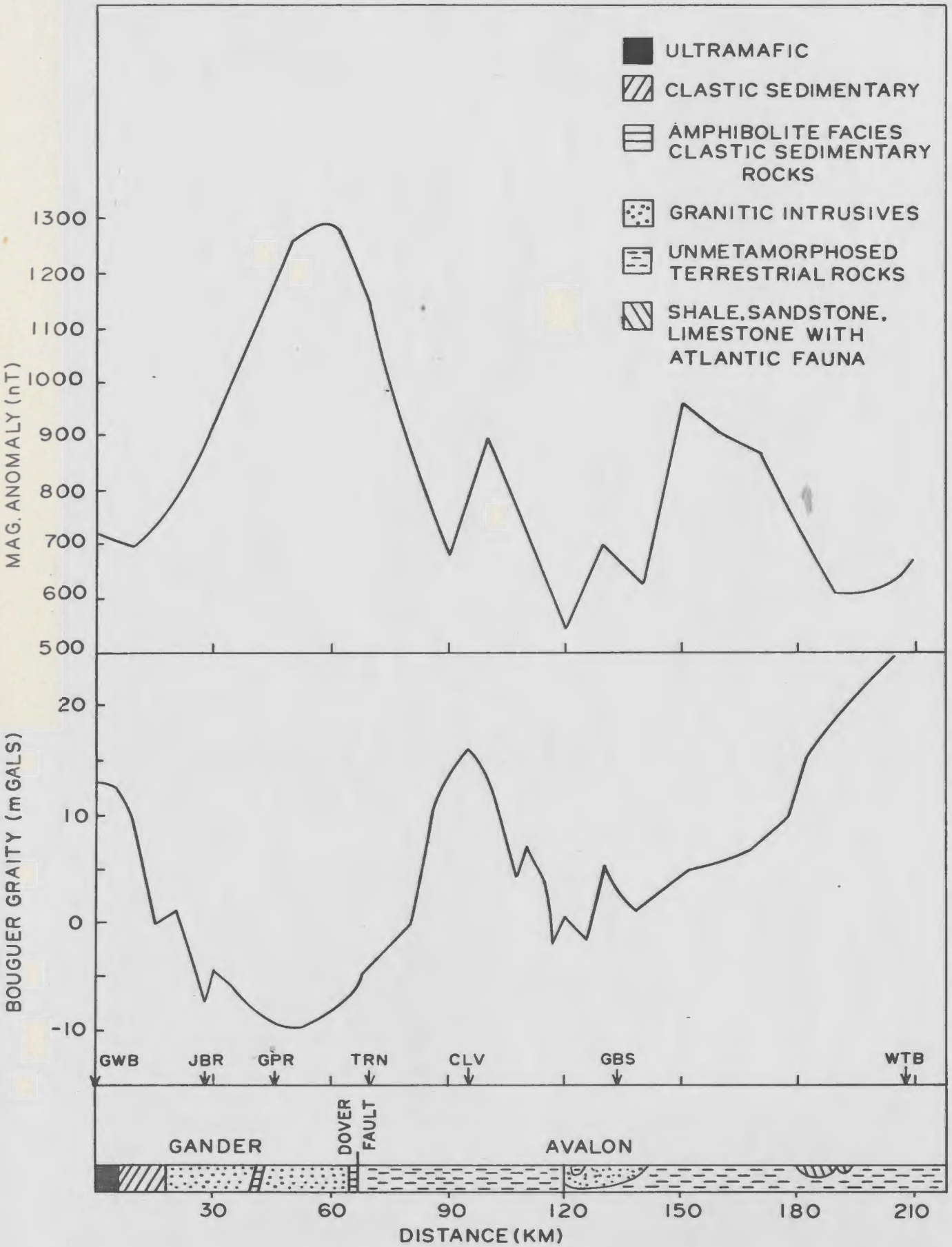

Fig. 5.2 Bouguer gravity anomaly and magnetic anomaly along the profile.

zone. In the Avalon zone, the gravity anomaly is mainly positive except at GBS. The positive anomalies in this region are explained by the presence of high density volcanic rocks under the Precambrian sediments and the negative anomalies are associated with the presence of granitic intrusions in the Avalon group (Miller, 1977).

The in phase and quadrature induction arrows at periods 40 sec, 10 sec, 4 sec and 1 sec are shown in the figures 5.3, 5.4, 5.5 and 5.6 respectively. The arrows indicate differences from the analogue model induction arrows of Hebert *et al*. (1983). These differences are large for all stations. The correlated nature of the signal leads to the conclusion that this is a result of correlated Z in the source signal. As this correlated component will be spatially uniform over the area of the survey, a mean at each period is subtracted from the arrows. The resulting differences are interpreted in terms of the local geology.

The in phase arrows at stations BLR and GWD point generally towards the geological boundary between the Dunnage and Gander zones at all frequencies indicating current concentrations along the boundary. A similar inference may be drawn for the stations JBR and GPR where the in phase arrows point towards the Dover fault which marks the eastern boundary of the Gander zone. The station TRN shows the effect due to the Dover fault and nearby coastline. At 40 sec period, the in phase arrow at the station points towards the nearest salt water. Incidentally, it is also the direction of several faults. However, at shorter periods (10 sec and 4 sec), the direction of the arrows gradually swings towards the Dover fault. At a period of 1 sec, the direction of

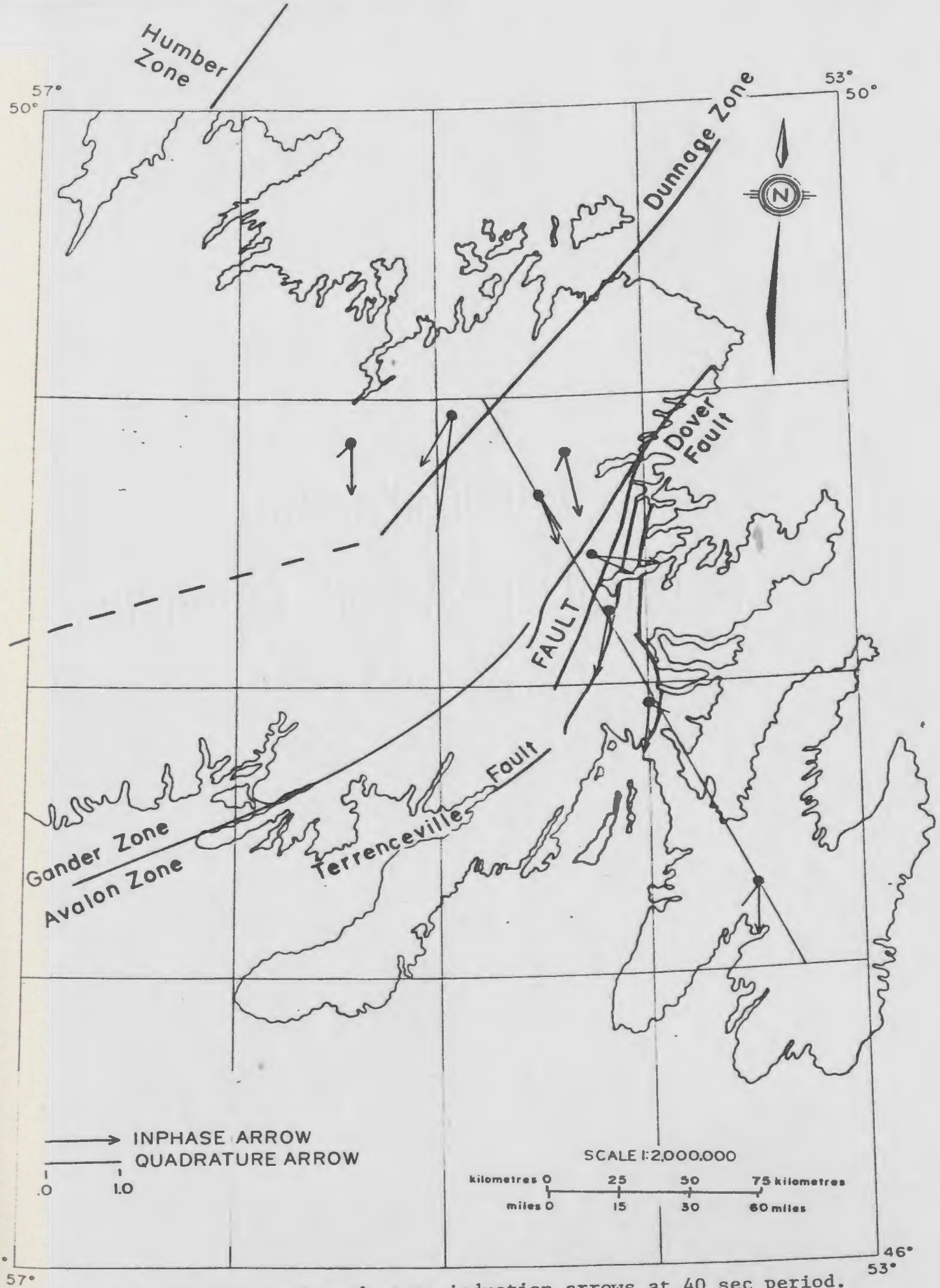

Fig. 5.3 In phase and quadrature induction arrows at 40 sec period.

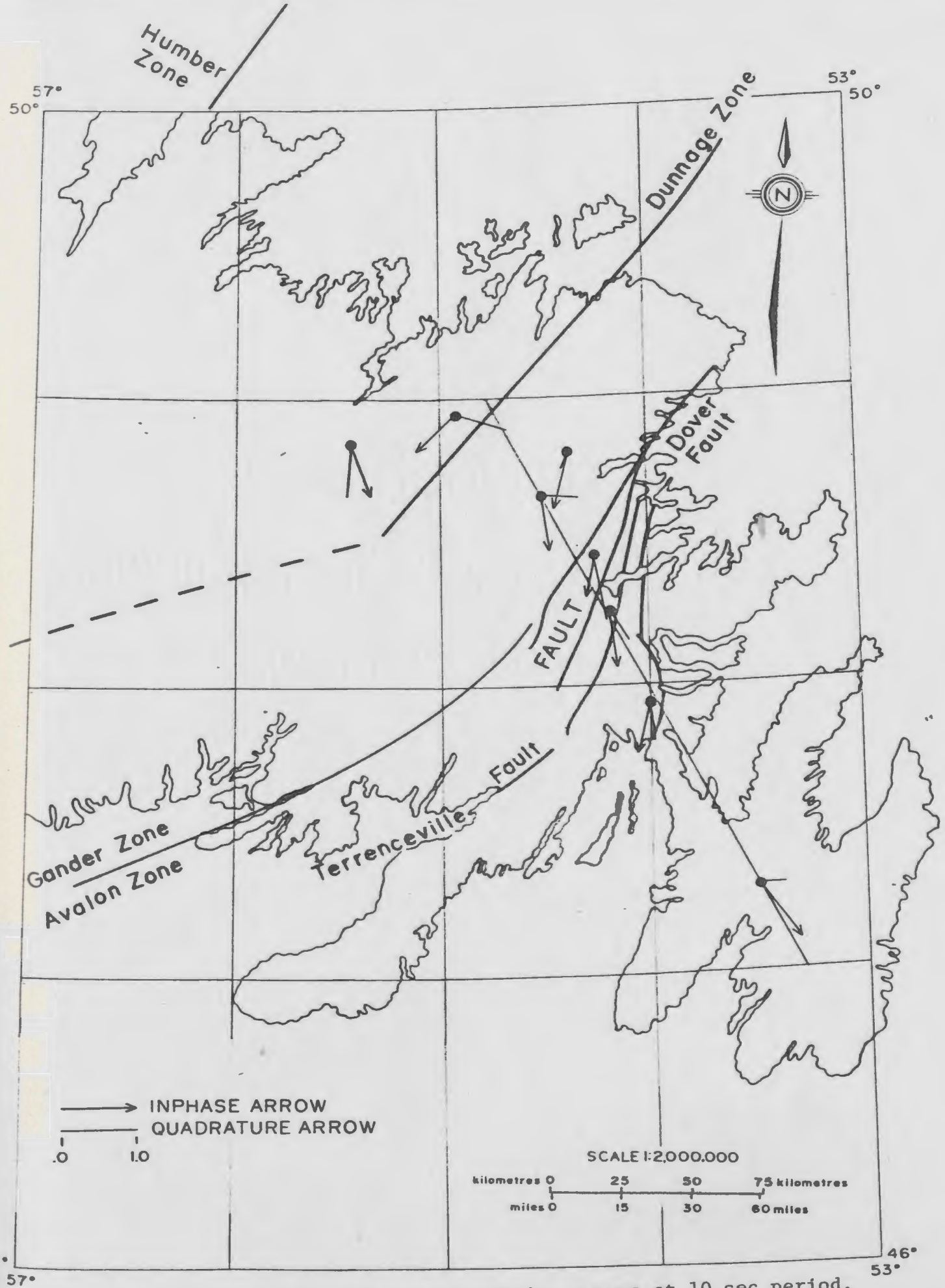

Fig. 5.4 In phase and quadrature induction arrows at 10 sec period.

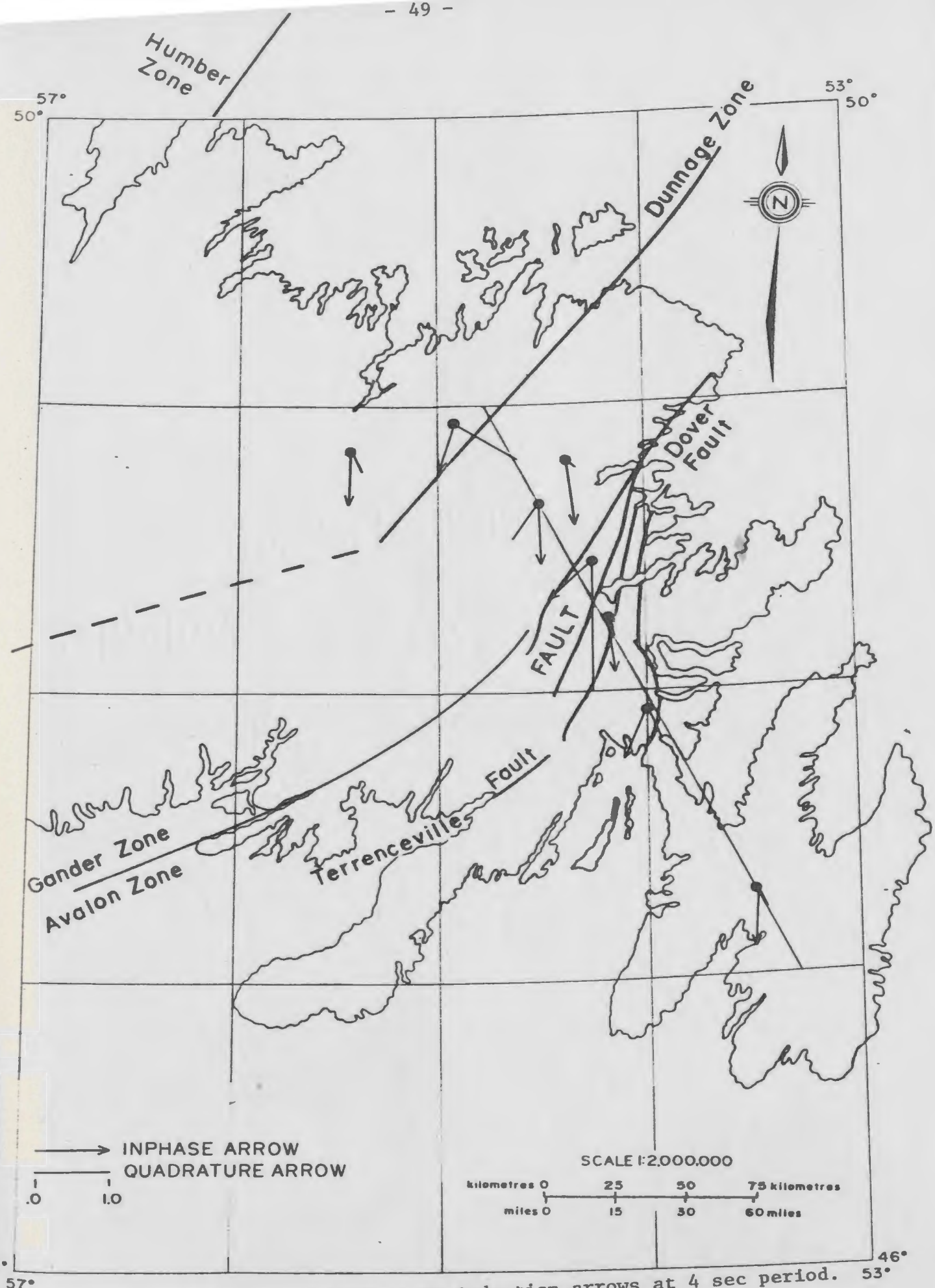

Fig. 5.5 In phase and quadrature induction arrows at 4 sec period.

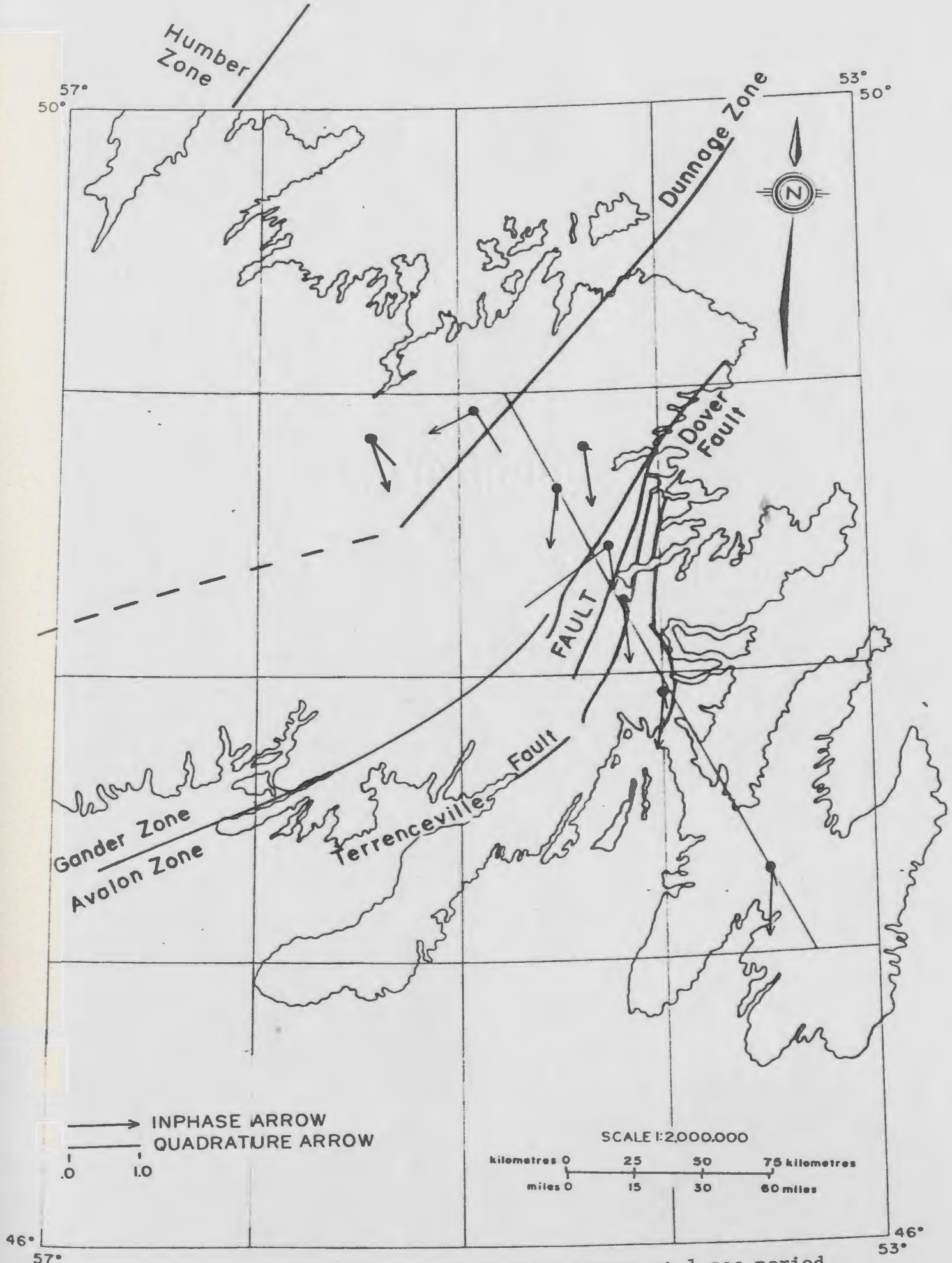

Fig. 5.6 In phase and quadrature induction arrows at 1 sec period.

the in phase arrow rotates to another fault line in the region but the large quadrature arrow still points towards the Dover fault. At 4 sec and 1 sec, the quadrature arrows just interchange directions with the in phase arrows. The behaviour of the in phase arrows at station CLV is fairly constant. They point towards the Terrenceville fault at all frequencies. The in phase arrows at WTB and GBS point towards the sea.

Current concentrations along the fault zones may be associated with one or other of the following causes. Deep fault zones are associated with several geophysical and geochemical phenomena such as fracturing of rocks, metamorphism, cataclasm, serpentinization and magma penetration all of which greatly reduce rock resistivity (Volarovich and Parkhomenko, 1976). Magmatism as a cause is eliminated in Newfoundland. Camfield and Gough (1977) mention that saline water may contribute to the high conductance in fault zones. Since Newfoundland is surrounded by sea, this is a plausible cause for the enhanced conductivity in the fault zones. The concentration of currents along geological boundaries can be explained by the presence of extensive hydrous mineralization, such as amphibolites and serpentinites (Law and Riddihough, 1971). There is ample geological evidence for hydrous mineralization in eastern Newfoundland and this possibility is further investigated.

If the anomalous field at a station is considered to be the resultant of the fields due to the underlying structure and the coast effect, then a simple vector subtraction of the coast effect induction arrows from the observed induction arrows would result in a difference arrow representing induction due to the underlying anomalous structure. As a first order approximation, the mutual inductance between the ocean and the inland conductor is ignored,

allowing modelling of difference arrows. Figures 5.7 and 5.8 show the plots of in phase difference arrows for periods 40 sec and 10 sec respectively. The coast effect induction arrows are taken from Hebert *et al.* (1983).

At 40 sec period (fig. 5.7), WTB shows a very small difference arrow pointing towards the isthmus of Avalon whereas the direction of the arrow at GBS is towards Placentia Bay. This indicates a leakage of current through the isthmus which acts as a narrow land barrier between Trinity Bay and Placentia Bay. CLV continues to point towards the Terrenceville fault at both 40 sec and 10 sec periods. The arrow at TRN does not change direction at 40 sec period, but at 10 sec period it points directly towards the Dover fault. The direction of the arrows at JBR and GPR at the period of 40 sec are away from the geological boundary at the Dover fault and point southwest towards the Gander Zone. At 10 sec period, they rotate further clockwise and point towards the centre of the Gander zone. This is a clear indication of an anomalous conductivity distribution under the crustal layers of the Gander zone.

The anomaly associated with the Gander zone has been recognized for the last few years and several researchers (Wright and Cochrane, 1980; Haworth *et al.*, 1978; Miller and Weir, 1982) have proposed models to interpret the anomaly. The model suggested by Wright and Cochrane (1980) is a descending lithospheric slab embedded

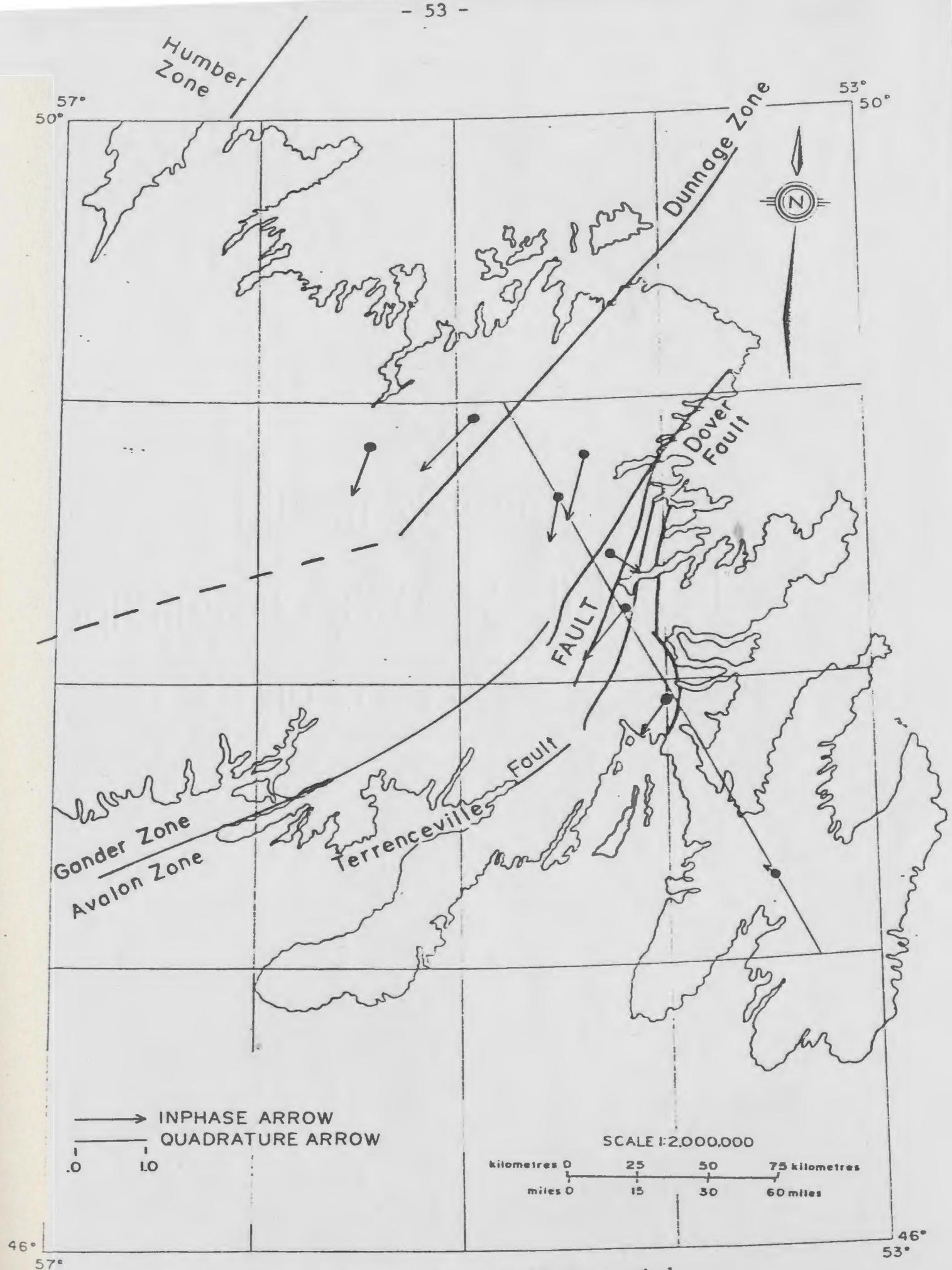

Fig. 5.7 In phase difference arrow at 40 sec period.

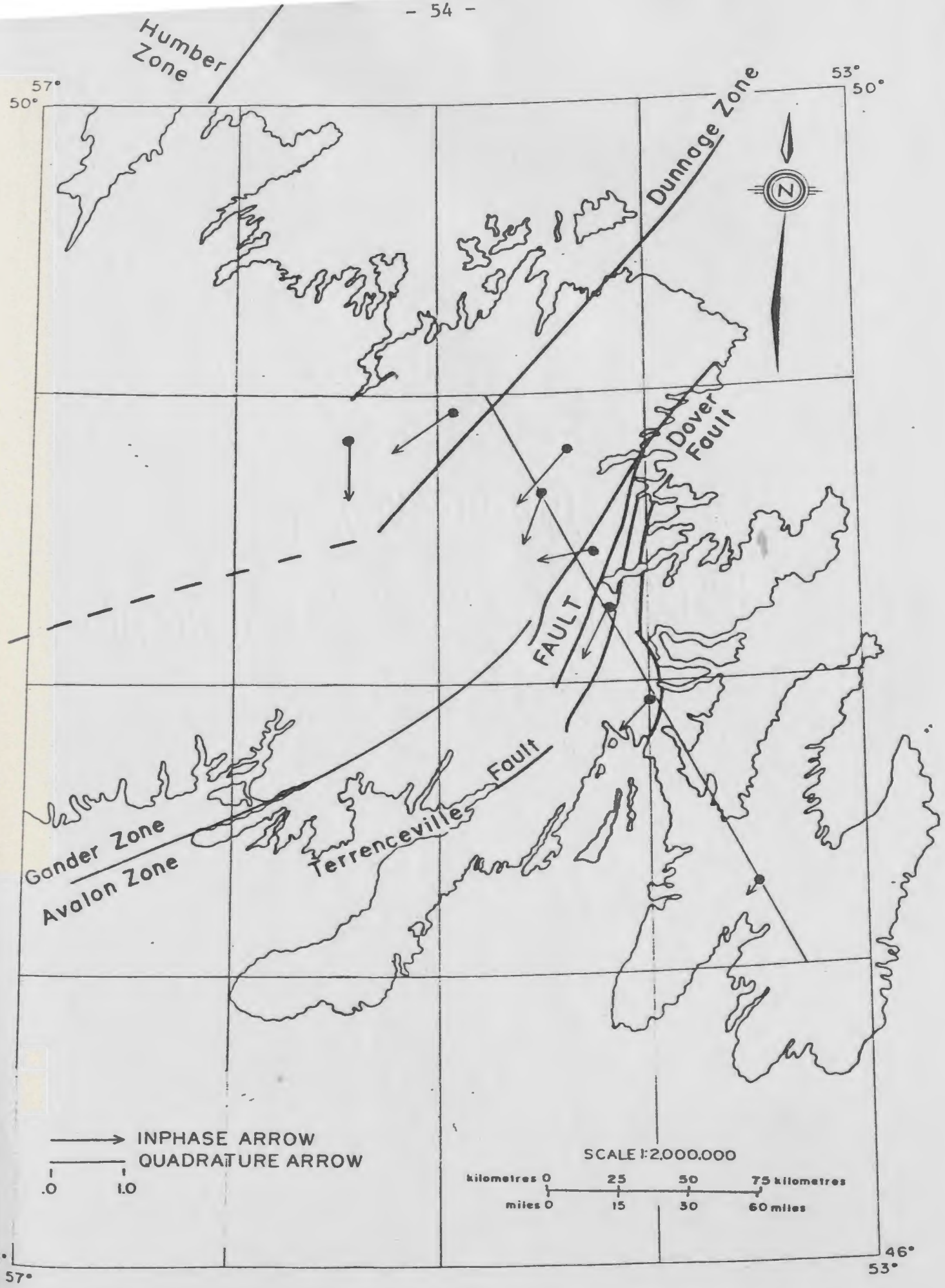

Fig. 5.8 In phase difference arrow at 10 sec period.

in the crust and upper mantle following east-dipping subduction under the Gander-Avalon boundary. Miller and Weir's (1982) model consists of an obducted ophiolitic slice placed on the Gander group at the time of Paleozoic subduction and burried by subsequent sedimentation. None of the above models are uniquely established. Therefore, these models and others are investigated in the light of the present observations.

5.2 Quantitative interpretation

In order to simulate the observed geomagnetic induction anomaly mentioned in section 5.1, a two-dimensional transmission line modelling technique is followed. Figure 5.9 displays in phase single station difference transfer function amplitudes resolved along the profile at 40 sec and 15.87 sec periods respectively. Station BLR is omitted from the profile since it lies in a different geological environment of the Dunnage zone. The upper portion of a crustal slab is modelled as a series of blocks ranging in width 5 km and 15 km on a 25 × 30 grid. The models have four layers including an air layer 200 km thick above the surface. The Cantwell-McDonald conductivity distribution (Madden and Swift, 1969) is used as a layered sequence for the modelling. Deviations from this gross Earth model are necessiated in order to obtain a best fit to the observed arrows. The resistivity of the conductive slab is taken as 25 Ω-m. As the observations indicate leakage of currents through the isthmus of Avalon, a conductive block of pseudo-resistivity of 50 Ω-m is assumed under the isthmus. The modelling constraints are based on the vertical

difference transfer functions along the profile which display relatively low amplitudes at TRN, high amplitudes on both sides of it and gradually decay with distance from the TRN over the period range 40 sec and 15.87 sec respectively (see figure 5.9). However, this feature gradually disappears at higher frequencies and will not be shown here.

Three different models are investigated to study the physical processes involved and conductivity distribution necessary for the observed anomaly in the area. These are: an east-dipping subduction under the Gander-Avalon zone; an obducted ophiolitic slice and a west-dipping subduction. The models are described in the following pages.

The first model is the east-dipping subduction model. A dipping conductive slab with resistivity of 25 Ω-m is modelled on 25 × 30 grid under the Avalon zone between TRN and CLV and extended 22 km into the Avalon zone. After running a large number of models for different depths, a good fit is obtained by placing a slab of 2 km thickness, 22 km long at a depth of 5 km under the Avalon zone. Figure 5.9 displays the model derived transfer function amplitudes versus distance from GWD along with the observed amplitudes for the periods 40 sec and 15.87 sec. This model shows a reasonably good agreement with the transfer functions on both sides of TRN and also with GPR at 40 sec. However, it does not quite match with the amplitude at GWD and WTB which are situated at the two ends

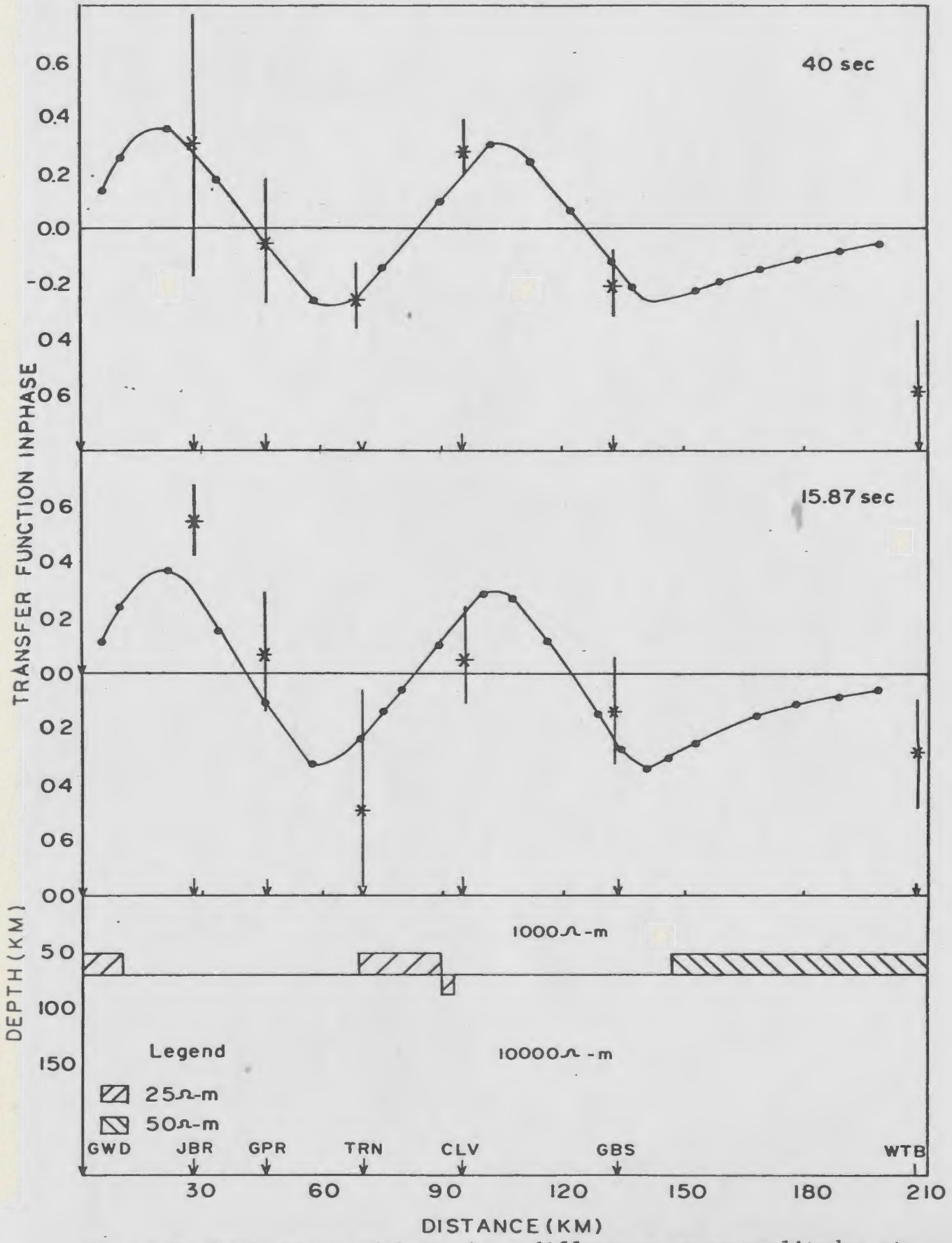

Fig. 5.9 Subduction model in phase difference arrow amplitudes at 40 sec and 15.87 sec period along the profile. The stars are the observed in phase difference arrow amplitudes projected onto the profile.

of the profile. The difference between the model and the observed parameters becomes larger at higher frequencies. This is may be due to contamination of observed transfer functions by the coherent noise and/or inhomogeneities in the near-surface crustal section. Except for WTB, the model transfer functions agree with the observed to within the limit of error.

For the second model, the same resistivity values and same number of grid points are used to model a slab of conductive material under the Avalon zone. First, a slab of the same length, thickness and depth as the first model is investigated to fit the observed values. It is found that the calculated transfer functions are too low to fit the data. Gradually the thickness and length of the slab are adjusted to fit the constraints of the model. A best fit is obtained for a slab of 2.5 km thickness, 28 km length at a depth of 5 km under the surface of the Avalon zone. Figure 5.10 shows the model calculated and observed transfer function amplitudes plotted against distance. As observed from the figure, this model also shows a very good agreement with the observed values at 40 sec and 15.87 sec periods.

The third model attempted is based on the hypothesis of west-dipping subduction in the area. Although there is no published evidence supporting west-dipping subduction in eastern Newfoundland, it is interesting to determine how a west-dipping subduction model compares

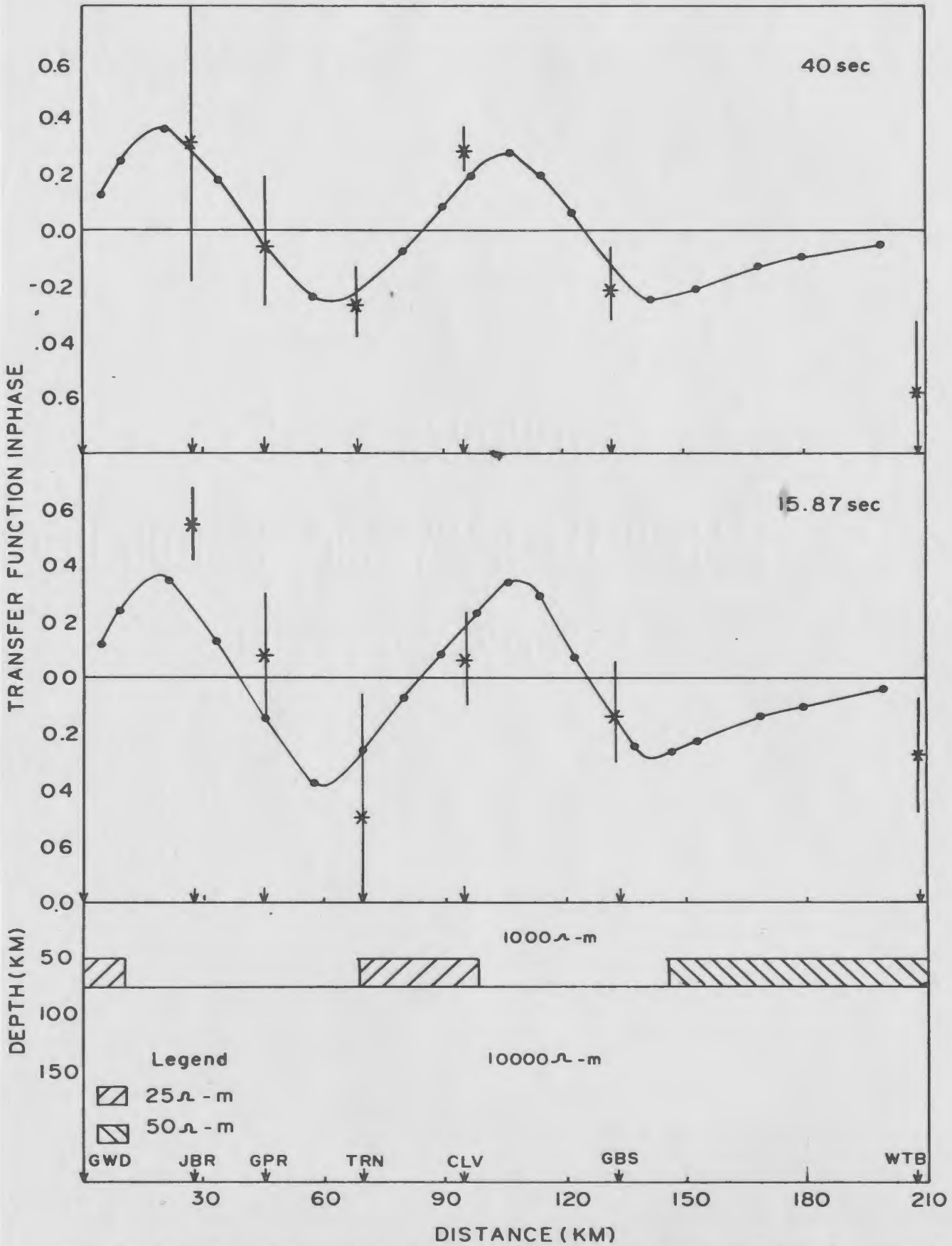

Fig. 5.10 Obduction model in phase difference arrow amplitudes along the profile at 40 sec and 15.87 sec periods. The stars are the observed in phase difference arrow amplitudes projected onto the profile.

to the observations. The layer resistivities for this model are the same as for the previous models. Assuming that the subduction zone lies under the western boundary of the Gander zone, several models were tested in the computer. None of them give a good fit to the observed data. Then, several models based on the hypothesis that a west-dipping zone lies under the Gander-Avalon boundary were investigated. They are found inconsistent with the observed data and therefore are not shown in the thesis.

One must point out that the actual geophysical phenomenon responsible for the observed anomaly in the area may be very complex in comparison to model descriptions. However, on the basis of the above analysis the first two models fit the observations quite well and they are equally geologically consistent.

CHAPTER 6

SUMMARY AND CONCLUSIONS

Geomagnetic induction studies in eastern Newfoundland in the period range 40 sec to 1 sec have revealed some interesting features regarding the anomalous conductivity distribution in the area. Two main aspects of this study are, the behaviour of the induction arrows at an intermediate frequency range 0.025 Hz to 1.0 Hz and the nature of response of the transfer functions to the near surface features. The directions of the in phase induction arrows consistently show that current concentrations in the Gander-Avalon zone are mainly associated with geological boundaries and faults. The in phase arrows at BLR, GWD, JBR, GPR, TRN and CLV display this behaviour (figures 5.3-5.6). Only at two stations WTB and GBS do the arrows strongly indicate current concentrations in the saline water of the Bay, which is a good conductor in comparison to the volcanics and Precambrian sedimentary rocks of the Avalon zone. Quadrature arrows, in general, are very large and are not well understood. This may be due to large near-surface inhomogeneities in the crustal rocks reflecting the complex geology common in Newfoundland or it could be an indication of coherent normal 'Z' in the vertical field records.

The signature of the inland anomaly in the observed data has been separated from the superimposed coast effect by applying difference arrow analysis technique (section 5.1). The assumption in this analysis is that the mutual inductance between the coast effect and

the inland conductor is small and can be neglected as a first-order approximation. The interpretation and conclusions in this thesis are based on the validity of the above assumption. This technique of analysis is also applied by Hebert *et al.* (1983).

The difference arrow analysis has brought out two important features of the area of study. First, the directions of the in phase difference induction arrows at WTB and GBS at 40 sec period (fig. 5.7) show a reversal indicating that there is a leakage of current through the isthmus of Avalon. This effect is represented in the models by a pseudo-conductivity of 0.02 S/m, the average conductivity of surface water and sea water. The second and the most important feature it has brought out is a zone of high conductivity under the Gander zone near Gander Lake. The arrows at JBR and GPR (figures 5.7 and 5.8) point toward this conductor. Two-dimensional modelling analysis places the conductor between the stations TRN and CLV. Two models, an east-dipping subduction zone and an obduction model agree equally well with the observed transfer functions. Both the models tentatively assign a conductivity of 0.04 S/m to the conductor. It is hypothesized that such a good conductor in the Gander Avalon boundary is a remnant oceanic fossil lithospheric slab embedded in the crust following a past subduction related to the closure of the proto-Atlantic ocean. There is ample evidence supporting this conjecture (Haworth *et al.*, 1978; Wright and Cochrane, 1980; Miller and Weir, 1982). The model of east-dipping subduction places the slab at a depth of 5 km

and dipping eastward (figure 5.9). The obduction model emplaces the slab at the same depth between the stations TRN and CLV and extended laterally 28 km into the Avalon zone (figure 5.10).

Although the two models differ in length of the slab under the Gander-Avalon boundary, both of the models assign the same conductivity value (0.04 S/m) to the slab. There are no reported direct experimental measurements of true conductivity of such old oceanic crustal materials at the appropriate temperature and pressure. However, Volarovich and Parkhomenko (1975) and Greenhouse and Bailey (1981) have discussed the conductivity of hydrous minerals. In oceanic crustal materials, serpentinites and amphibolites are very common (Christensen and Salisbury, 1975) and they are known to be good conductors in presence of free water or water of hydration (see section 1.5). At shallow crustal depths the role of free water could be prominent and free water can enhance the conductivity in two ways. First, free water supports electrolytic conduction through the pores and fractures of the material. Secondly, it creates certain hydrous minerals that are relatively good conductors (Greenhouse and Bailey, 1981). A small change in the abundance of these hydrous minerals could profoundly change the conductivity of the rocks which may vary in a wide range between 0.01 to 1.0 S/m (Volarovich and Parkhomenko, 1975).

A model study investigating the possibility of a west-dipping subduction zone was also carried out. The model results do not show any substantive agreement with the observations.

As observed from the figures 5.9 and 5.10, the subduction and the obduction model show good agreement with the observed data. For the present distribution of stations, method of analysis followed to separate the signature of the inland anomaly from the observed data and the technique of modelling used to portray the subsurface conductivity distribution, it is not possible to distinguish which model is more appropriate in describing the anomaly pattern in the area. A denser network of stations with three-dimensional modelling techniques or a magnetotelluric measurement in the high frequency range could resolve this question.

Irrespective of the dip and lateral extension of the conductor under the Gander-Avalon zone, the results indicate that there is a near-surface, north-east trending high conductivity zone running between the stations TRN and CLV and extended a few kilometers inside the Avalon zone. This conductor may be an extension of the same structure near Gander Lake as identified by Miller and Weir (1982) by a gravity-magnetic survey. A dipping conductive fossil lithospheric slab under the Gander-Avalon boundary was also suggested by Wright and Cochrane (1980) on the basis of geomagnetic induction measurements.

It is a matter for speculation if the same structure running from the Carmanville melange is dipping south-eastward. This type of conductivity anomaly may also be investigated in the context of the setting of the northern Appalachians (Cochrane and Hyndman, 1974).

The transfer functions at WTB do not fit at all with any one of the above discussed models at any frequency. Since WTB is situated at the end of the profile and there are inadequate data in that area, no attempt has been made to model the response independently. May be, it is an indication that the coast effect calculated by Hebert *et al*. (1983) is over estimated.

BIBLIOGRAPHY

Bailey, R.C. 1973. Global geomagnetic sounding. Phys. Earth Planet. Int., 7, 234-244.

Bailey, R.C., Edwards, R.N., Garland, G.D., Kurtz, R.D., and Pitcher, D. 1974. Electrical conductivity studies over a tectonically active area in eastern Canada. J. Geomag. Geoelectr., 26, 125-146.

Bailey, R.C. 1977. Electromagnetic induction over the edge of a perfectly conducting ocean. Geophys. J. Roy. Astr. Soc., 48, 385-392.

Banks, R.J. 1973. Data processing and interpretation of geomagnetic deep sounding. Phys. Earth Planet. Int., 7, 339-348.

Bath, M. 1974. Spectral analysis in Geophysics. Elsevier Scientific Publishing Company, p. 95.

Bendat, J.S., and Piersol, A.G. 1966. Measurement and analysis of random data. John Wiley & Sons Inc., N.Y., London, Sydney, p. 301.

Blackwood, R.F., and Kennedy, M.J. 1975. The Dover fault; western boundary of the Avalon zone in northeastern Newfoundland. Can. J. Earth Sci., 12, 320-325.

Blackwood, R.F. 1976. The relationship between the Gander and Avalon zones in the Bonavista Bay region, Newfoundland. M.Sc. Thesis, Memorial University of Newfoundland, St. John's.

Brewitt-Taylor, C.R. 1975. A model for the coast effect. Phys. Earth Planet. Int., 10, 151-158.

Brewitt-Taylor, C.R. 1976. A model for the seafloor coast effect in H-polarization. Phys. Earth Planet. Int., 13, 9-14.

Camfield, P.A., and Gough, D.I. 1977. A possible Proterozoic plate boundary in North America. Can. J. Earth Sci., 14, 1229-1238.

Christensen, N.I., and Salisbury, M.H. 1975. Structure and constitution of the lower oceanic crust. Rev. Geophys. Space Phys., 13, 57-86.

Cochrane, N.A., and Hyndman, R.D. 1970. A new analysis of geomagnetic depth sounding data from western Canada. Can. J. Earth Sci., 7, 1208-1218.

Cochrane, N.A. 1972. Geomagnetic and geoelectric variations in Atlantic Canada. Ph.D. Thesis, Dalhousie University.

Cochrane, N.A., and Hyndman, R.D. 1974. Magnetotelluric and magnetovariational studies in Atlantic Canada. Geophys. J. Roy. Astr. Soc., 39, 385-406.

Cochrane, N.A., and Wright, J.A. 1977. Geomagnetic sounding near the northern termination of the Appalachian system. Can. J. Earth Sci., 14, 2858-2864.

Cooley, J.W., and Tukey, J.W. 1965. An algorithm for the machine calculations of complex Fourier series. Mathematics of Computation, 19, 297-307.

d'Erceville, I., and Kunetz, G. 1962. The effect of a fault on the earth's natural electromagnetic field. Geophys., 35, 651-665.

Dosso, H.W. 1966. Analogue model measurements for electromagnetic variations near a coast line. Can. J. Earth Sci., 3, 917-936.

Dosso, H.W., Nienaber, W., Wright, J.A., Greenhouse, J.P., and Bailey, R.C. 1980. An Analogue model study of electromagnetic induction in the eastern coastal region of North America. Phys. Earth Planet. Int., 23, 13-30.

Dyck, A.V., and Garland, G.D. 1969. A conductivity model for certain features of the Alert anomaly in geomagnetic variations. Can. J. Earth Sci., 6, 513-516.

Edwards, R.N., Law, L.K., and White, A. 1971. Geomagnetic variations in the British Isles and their relation to electric current in the ocean and shallow seas. Phil. Tran. Roy. Soc. Lond. Ser A, 270, 289-323.

Everett, J.E., and Hyndman, R.D. 1967. Geomagnetic variations and electrical conductivity structures in south western Australia. Phys. Earth Planet. Int., 1, 24-34.

Feldman, I. 1976. On the nature of conductive layers in the Earth's upper mantle. In Geoelectric and Geothermal Studies. Edited by A. Adam. Akademiai Kiado, Budapest, pp. 721-730.

Fischer, G.,Schnegg, P.A.,and Usadel, K.D. 1978. Electromagnetic response of an ocean-coast model to E-Polarization induction. Geophys. J. Roy. Astron. Soc., 53, 599-616.

Frazer, M.C. 1974. Geomagnetic deep sounding with arrays of magnetometers. Rev. Geophys. Space Phys., 12, 401-420.

Geyer, R.G. 1972. The effect of dipping contact on the behaviour of the electromagnetic field. Geophys., 37, 337-350.

Gough, D.I. 1973. The geophysical significance of geomagnetic variation anomalies. Phys. Earth Planet. Int., 7, 379-388.

Gough, D.I., de Beer, J.H.,and Van Zijl, J.S.V. 1973. A magnetometer array study in southern Africa. Geophys. J. Roy. Astron. Soc. 34, 421-433.

Greenhouse, J.P.,and Bailey, R.C. 1981. A review of geomagnetic variation measurements in the eastern United States: implications for continental tectonics. Can. J. Earth Sci., 18, 1268-1289.

Gregori, G.P., and Lanzerotti, L.J. 1980. Geomagnetic depth sounding by induction arrow representation: a review. Rev. geophys. space phys., 18, 203-209.

Haworth, R.T., Lefort, J.P., and Miller, H.G. 1978. Geophysical evidence for an east-dipping Appalachian subduction zone beneath Newfoundland. Geology, 6, 522-526.

Haworth, R.T., and Keen, C.E. 1979. The Canadian Atlantic Margin: A passive continental margin encompassing an active past. Tectonophysics, 59, 83-126.

Hebert, D., Dosso, H.W., Nienaber, W., and Wright, J.A. 1983. Analogue model study of electromagnetic induction in the Newfoundland region. Phys. Earth Planet. Int. 31 (in Press).

Hermance, J.F. 1973. Processing of magnetotelluric data. Phys. Earth Planet. Int., 7, 349-364.

Hinich, M.J. 1967. Estimation of exponential power spectra. J. Acoust. Soc. Am., 42, 422-427.

Hyndman, R.D., and Hyndman, D.W. 1968. Water saturation and high electrical conductivity in the lower continental crust. Earth Planet. Sci. Letters, 4, 427-432.

Hyndman, R.D., and Cochrane, N.A. 1971. Electrical conductivity structure by geomagnetic induction at the continental margin of Atlantic Canada. Geophys.J., 25, 425-446.

Jones, R.H. 1965. A reappraisal of the periodogram in spectral analysis. Technometrics, 7, 531-542.

Jones, F.W.,and Price, A.T. 1970. The perturbation of alternating geomagnetic fields by conductivity anomalies. Geophys. J. Roy. Astr. Soc., 20, 317-334.

Kanasewich, E.R. 1975. Time sequence analysis in geophysics. The University of Alberta press, p. 41.

Kay, M. 1976. Dunnage melange and subduction of the protacadic ocean, Northeast Newfoundland. Geological Soc. America, special paper 175, 49.

Kennedy, M.J. 1976. South eastern margin of the Northeastern Appalachians: late precambrian orogeny on a continental margin, Geological Soc. America Bulletin, 87, 1317-1325.

Law, L.K., and Riddihough, R.P. 1971. A geographical relationship between geomagnetic variation anamolies and tectonics. Can. J. Earth Sci., 8, 1094-1106.

Lilley, F.E.M., and Arora, B.R. 1982. The sign convention for quadrature Parkinson arrows in geomagnetic induction studies. Rev. geophys. space phys., 20, 513-518.

Lines, L.R., Ainslie, B.A.,and Jones, F.W. 1973. Investigation of the coastal effect by three numerical models. J. Geomag. Geoelectr., 25, 63-73.

Madden, T.R., and Swift, C.M., Jr. 1969. Magnetotelluric studies of the electrical conductivity structure of the crust and upper mantle. AGU Monograph 13, The Earth's crust and upper mantle, p. 469.

McKerrow, W.S., and Cocks, L.R.M. 1977. The location of the Iapetus ocean suture in Newfoundland. Can. J. Earth Sci., 14, 488-495.

McKerrow, W.S., and Cocks, L.R.M. 1978. A lower paleozoic trench-fill sequence, New World Island, Newfoundland. Geological Soc. America Bull., 89, 1121-1132.

Miller, H.G., and Deutsch, E.R. 1978. The Bouguer anomaly field of the Notre Dame Bay area, Newfoundland with map No. 163. Earth Physics Branch, Ottawa, Gravity map series No. 163.

Miller, H.G., and Deutsch, E.R. 1973. A gravity survey eastern Notre Dame Bay, Newfoundland in earth symposium on off-shore eastern Canada, P.J. Hood (ed.). Geological Survey of Canada paper 71-23, 389-406.

Miller, H.G. 1977. Gravity zoning in Newfoundland. Tectonophysics, 38, 317-326.

Miller, H.G., and Weir, H.C. 1982. The northwest portion of the Gander zone - a geophysical interpretation. Can. J. Earth Sci. 19, 1371-1381.

Neves, A.S. 1957. The magnetotelluric method in two dimensional structures. Ph.D. Thesis, M.I.T., Cambridge, Massachusetts.

Nicholl, M.A., and Weaver, J.T. 1977. H-Polarization over an ocean edge coupled to the mantle by a conducting crust. Geophys. J. Roy. Astron. Soc., 49, 427-441.

Pajari, G.E., Jr., and Currie, K.L. 1978. The Gander Lake and Davidsville groups of northeastern Newfoundland: a re-examination. Can. J. Earth Sci., 15, 708-714.

Parkhomenko, E.I. 1967. Electrical properties of rocks. Plenum Press, N.Y.

Parkinson, W.D. 1959. Direction of rapid geomagnetic fluctuations. Geophys. J. Roy. Astr. Soc., 2, 1-14.

Parkinson, W.D., and Jones, F.W. 1979. The geomagnetic coast effect. Rev. geophys. space phys., 17, 1999-2015.

Porath, H., and Dziewonski, A. 1971. Crustal resistivity anomalies from geomagnetic deep sounding studies. Rev. Geophys. Space Phys. 9, 891-915.

Price, A.T. 1973. The theory of electromagnetic Induction. Phys. Earth planet. Int., 7, 227.

Rankin, D. 1962. The magnetotelluric effect on a dyke. Geophys., 27, 666-676.

Rikitake, T. 1966. Electromagnetism and Earth's Interior. Elsevier Publishing Company, N.Y.

Rooney, D. 1976. Magnetotelluric measurements across the Kenyan rift valley. Ph.D. Thesis, University of Edinburgh.

Salisbury, M.H., and Christensen, N.I. 1978. The seismic velocity structure of a traverse through the Bay of Islands ophiolitic complex, Newfoundland, an exposure of oceanic crust and upper mantle. J. geophys. Res.,,83, 805-817.

Schmucker, U. 1964. Anomalies of geomagnetic variations in the southwestern United States. J. Geomag. Geoelectr. 15, 193-221.

Schmucker, U. 1970. Anomalies of geomagnetic variations in the southwestern United States. Bull. Scripps. Inst. Oceanography, University of California, San Diego.

Sheridan, R.E.,and Drake, C.L. 1968. Seaward extension of the Canadian Appalachians. Can. J. Earth Sci., 5, 337-373.

Sims, W.E., and Bostick, F.X., Jr. 1969. Methods of magnetotelluric analysis: EGRL Technical Report no. 58. University of Texas, Austin.

Stewart, I.C.F. 1978. Teleseismic reflections and the Newfoundland lithosphere. Can. J. Earth Sci., 15, 175-180.

Strong, D.F., Dickson, W.L., O'Driscoll, C.F., Kean, B.F.,and Stevens, R.K. 1974. Geochemical evidence for eastward Appalachian subduction in Newfoundland. Nature, 248, 37-39.

Swift, C.M., Jr. 1967. A magnetotelluric investigation of an electrical conductivity anomaly in the South-Western United States. Ph.D. Thesis, M.I.T.; Cambridge, Massachusetts.

Tatrallyay, M. and Jones, F.W. 1974. The perturbation of geomagnetic fields by cylindrical structures. Geophys. J. Roy. Astro. Soc., 38, 449-477.

Telford, W.M., Geldart, L.P., Sheriff, R.E., and Keys, D.A. 1976. Applied Geophysics. Cambridge University Press, pp.500-631.

Tukey, J.W. 1967. Spectral Analysis of time series. Edited by B. Harris, pp. 25-46.

Volarovich, M.P., and Parkhomenko, E.I. 1976. Electrical properties of rocks at high temperatures and pressures. Geoelectric and Geothermal studies, KAPG, Geophysical Monograph, pp. 321-369.

Wait, J.R. 1962. Electromagnetic waves in stratified media. Pergamon Press, pp. 10-11.

Weaver, J.T. 1963. The electromagnetic field within a discontinuous conductor with reference to geomagnetic micropulsations near a coast line. Can. J. Phys., 41, 484-495.

Weaver, D.F. 1967. A geological interpretation of the Bouguer anomaly field of Newfoundland. Publication of Dominion Observatory, volume 35, No. 5, Ottawa.

Weir, H.C. 1971. A gravity profile across Newfoundland. M.Sc. Thesis, Memorial University of Newfoundland, St. John's, Nfld.

Weise, H. 1962. Geomagnetisches Tiefentellurik. Geophys. Pure Appl., 52, 83-103.

Williams, H. 1964. The Appalachians in Northeastern Newfoundland - A two sided symmetrical system. American J. Sci., 262, 1137-1158.

Williams, H. 1975. Structural succession, nomenclature, and interpretation of transported rocks in western Newfoundland. Can. J. Earth Sci., 12, 1874-1894.

Williams, H., and King, A.F. 1977. Geological development of the Appalachians. The Newfoundland J. of Geological Education, vol. 3, no. 1, 17-33.

Williams, H. 1979. Appalachian orogen in Canada. Can. J. Earth Sci., 16, 792-807.

Wright, J.A. 1969. The electromagnetic response of two dimensional structures, Gamma-7, Inst. Geophysik Meteorologic Tech. University, Braunschweig.

Wright, J.A., and Cochrane, N.A. 1980. Geomagnetic sounding of an ancient plate margin in the Canadian Appalachians. J. geomag. geoelect., 32, Supplement 1, 133-140.

APPENDIX A

Transfer Functions

The frequency response of the in phase and quadrature induction arrows and their azimuths are shown in figures A1 - A16. The angles are in degrees and are measured clockwise from geographical north. The error bars indicate scattering of the computed values within one standard deviation from a set of individual values.

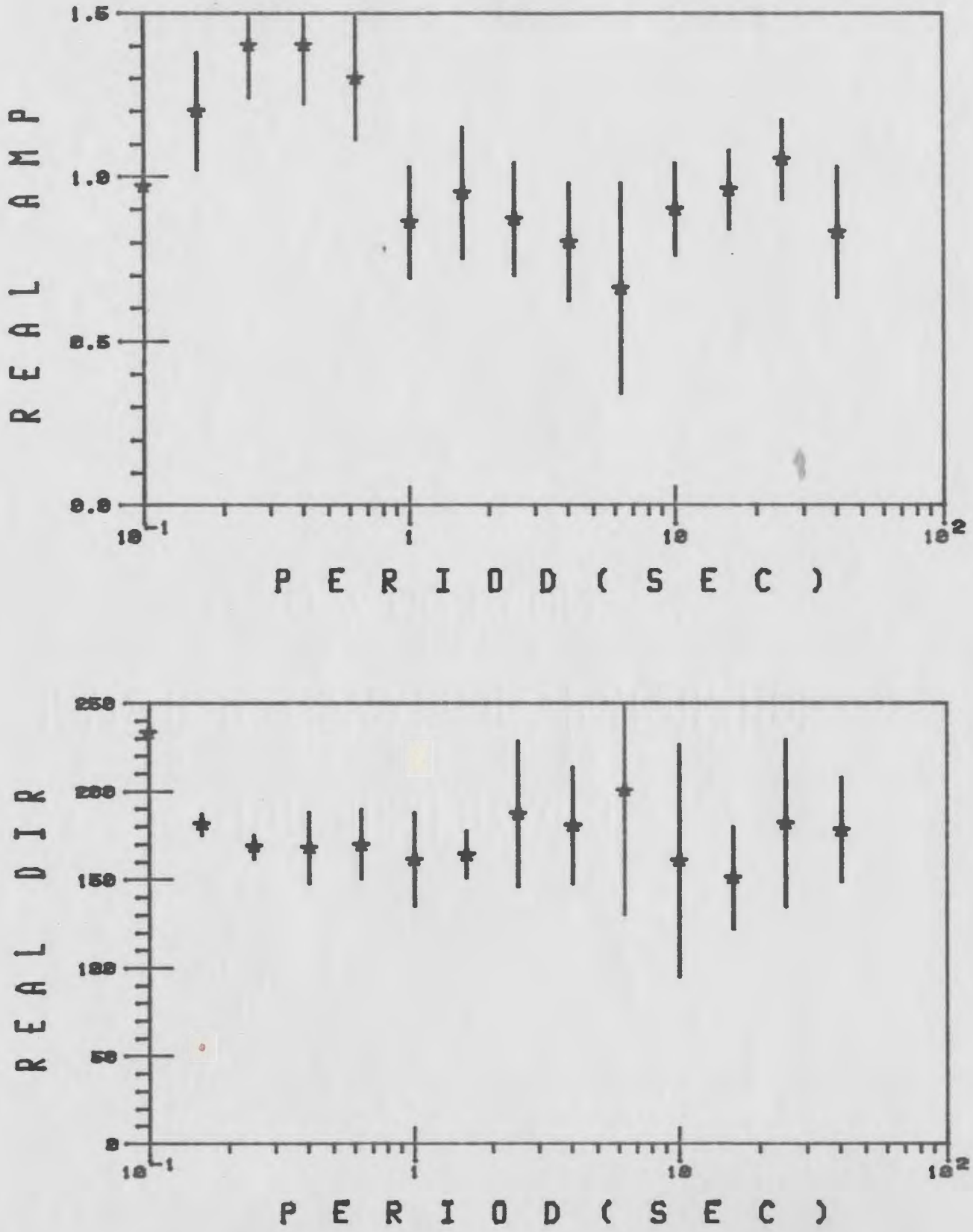

Fig. A1 Frequency and phase response of the real (in phase) arrows at BLR.

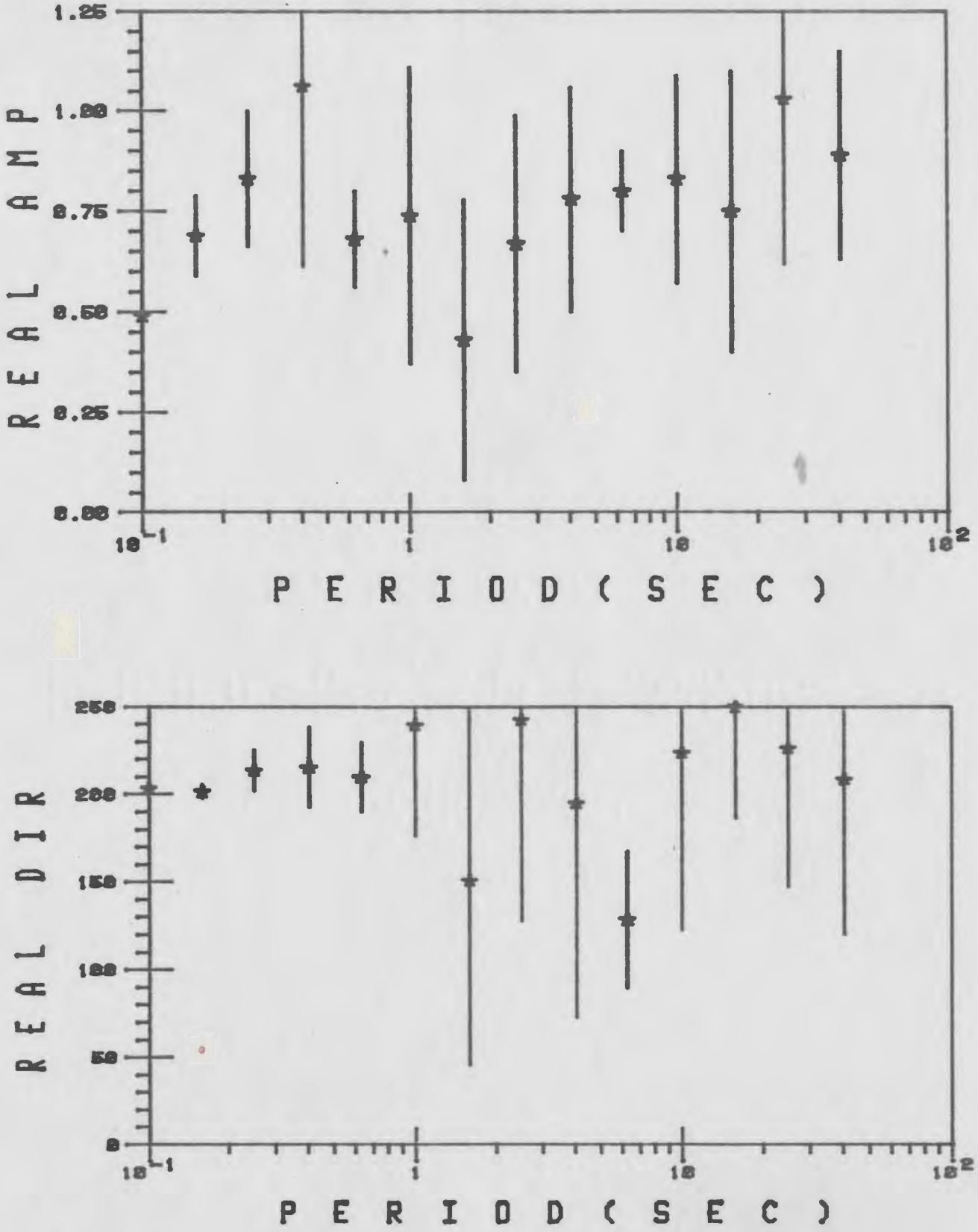

Fig. A2 Frequency and phase response of the real (in phase) arrows at GWD.

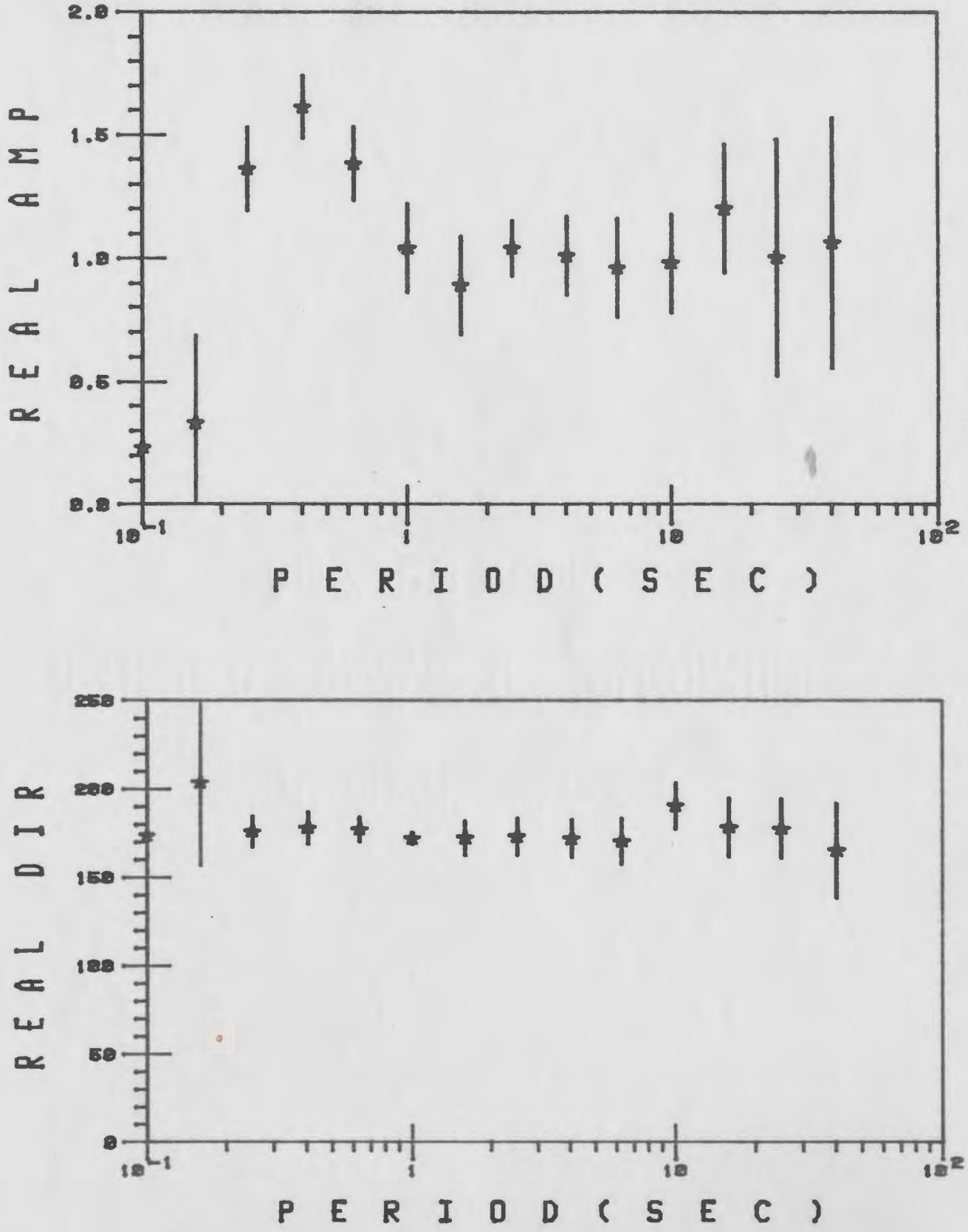

Fig. A3 Frequency and phase response of the real (in phase) arrows at JBR.

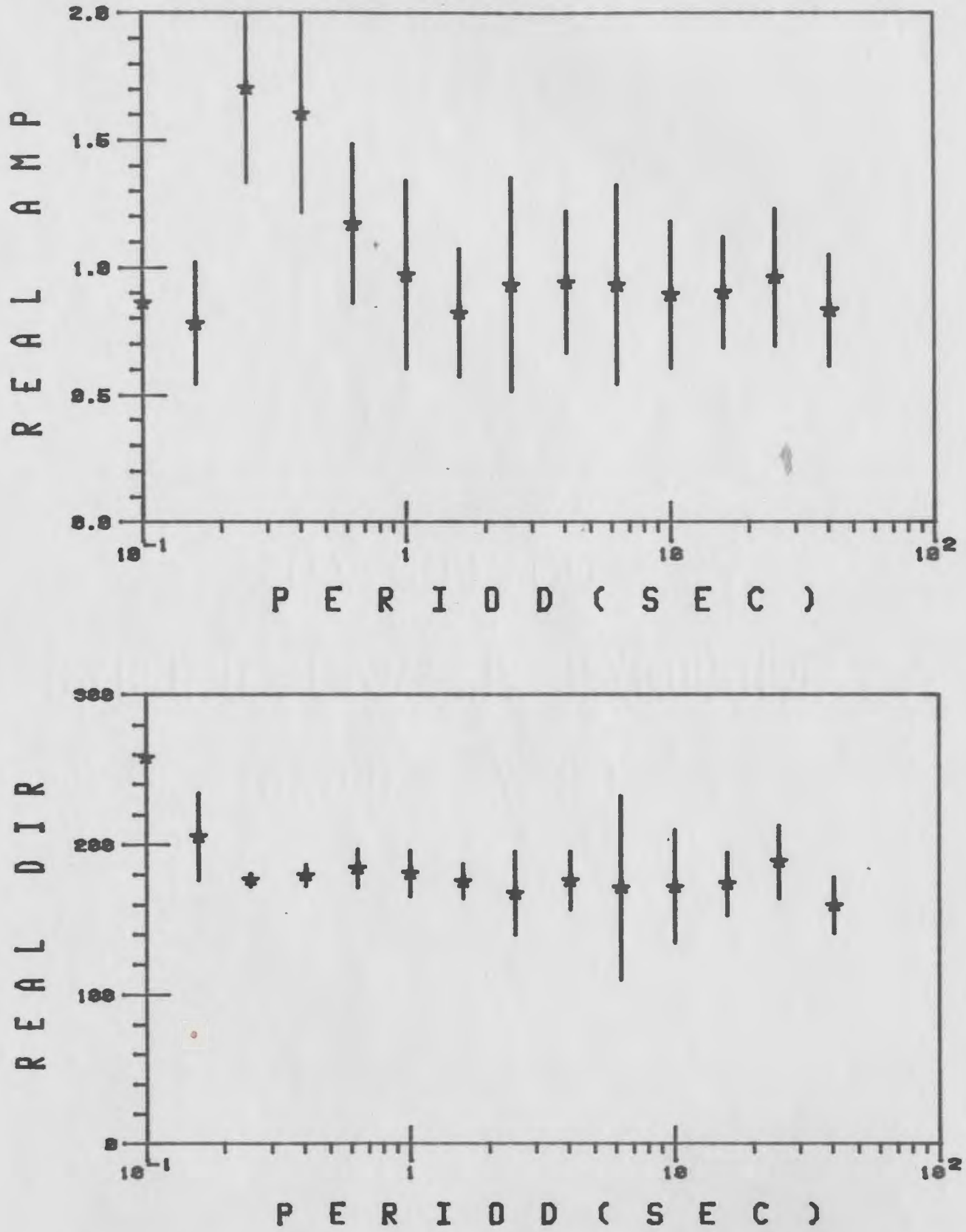

Fig. A4 Frequency and phase response of the real (in phase) arrows at GPR.

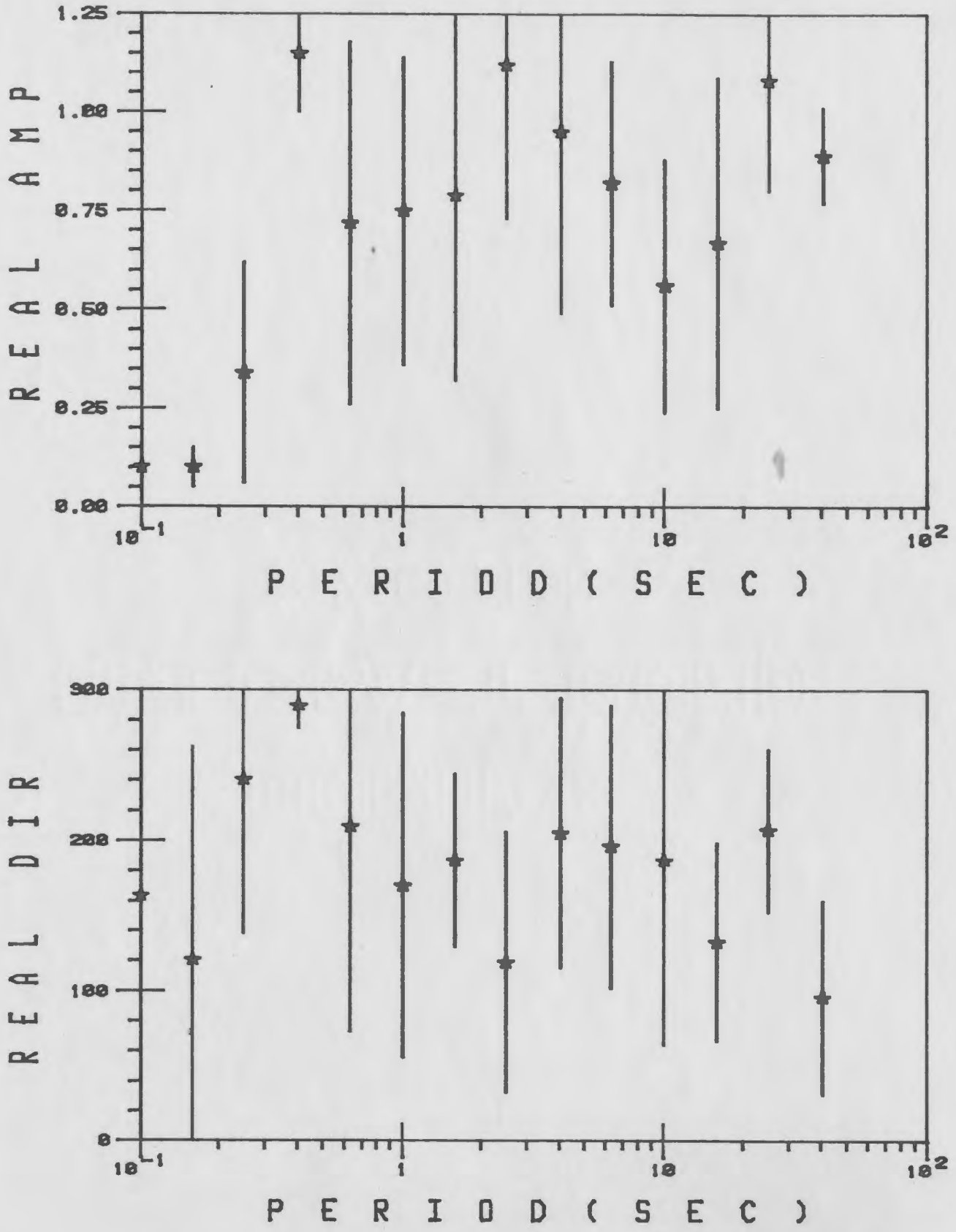

Fig. A5 Frequency and phase response of the real (in phase) arrows at TRN.

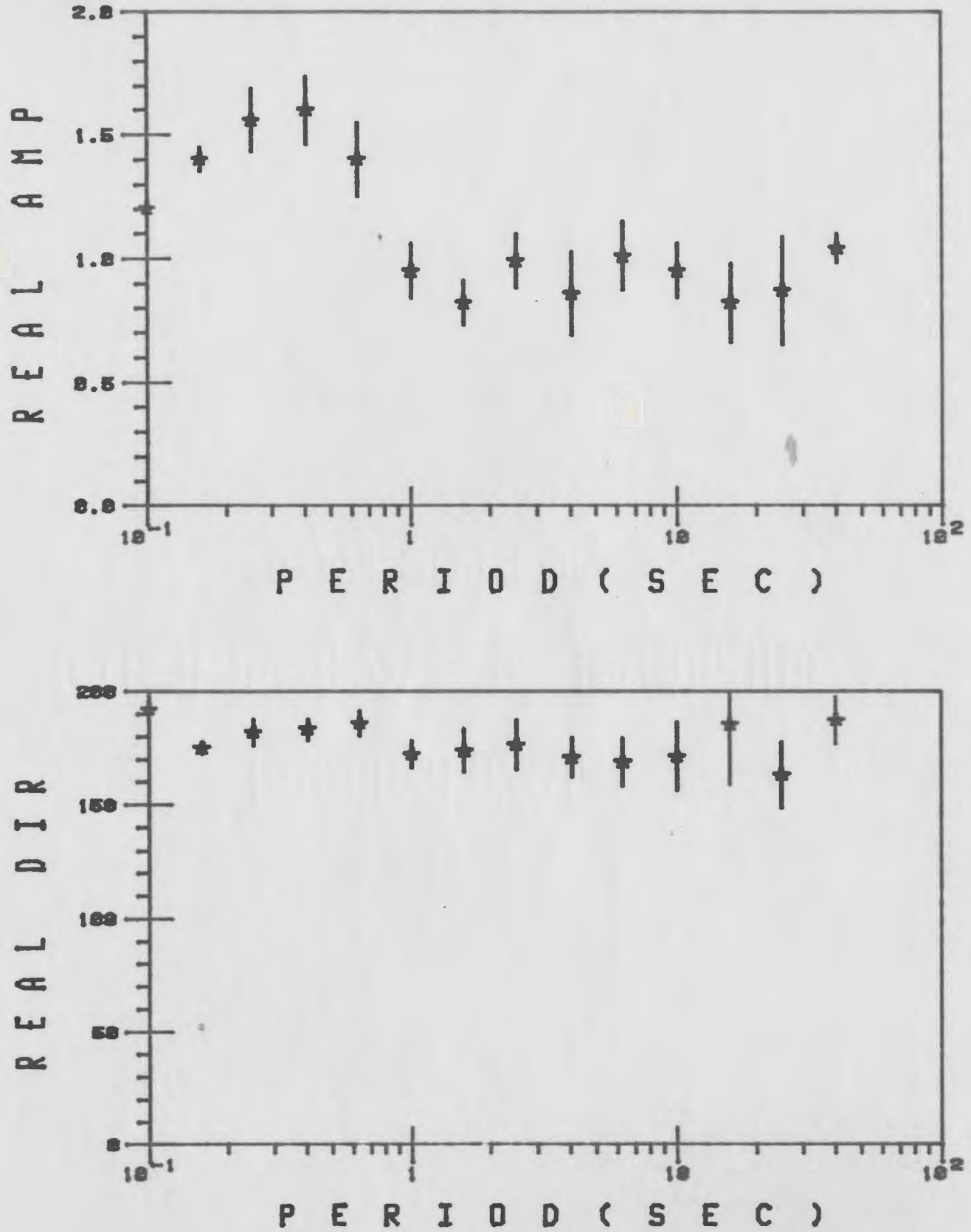

Fig. A6 Frequency and phase response of the real (in phase) arrows at CLV.

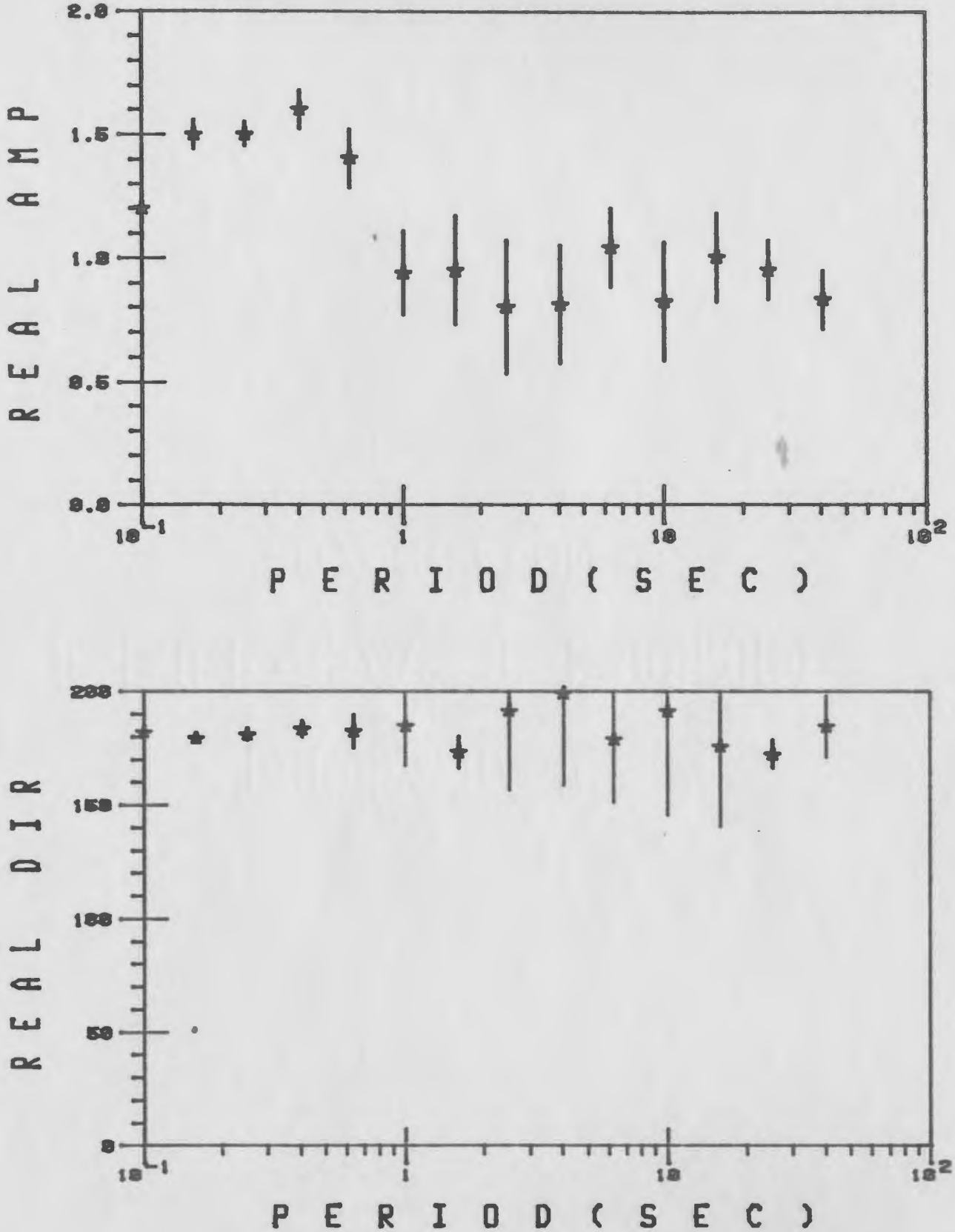

Fig. A7 Frequency and phase response of the real (in phase) arrows at GBS.

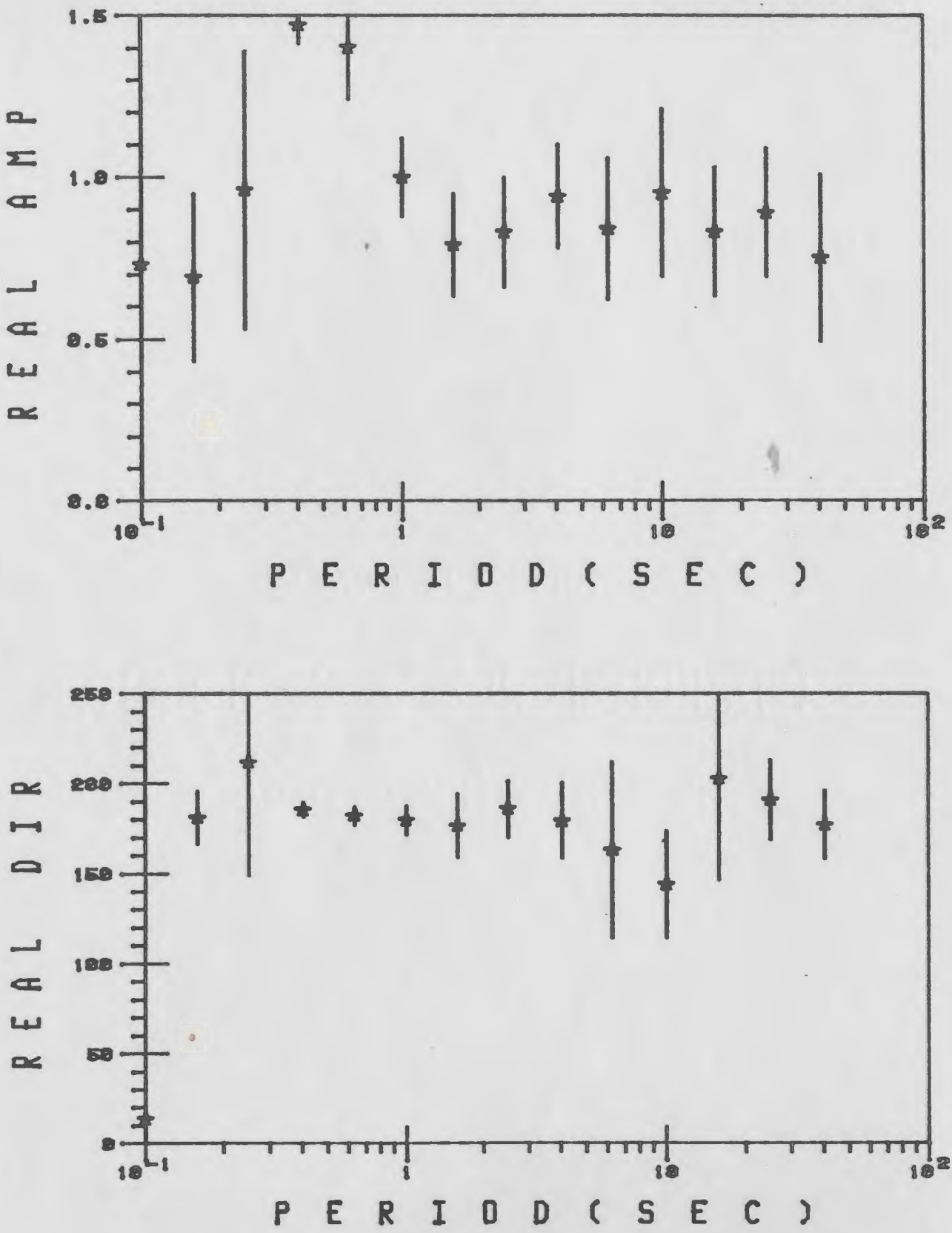

Fig. A8 Frequency and phase response of the real (in phase) arrows at WTB.

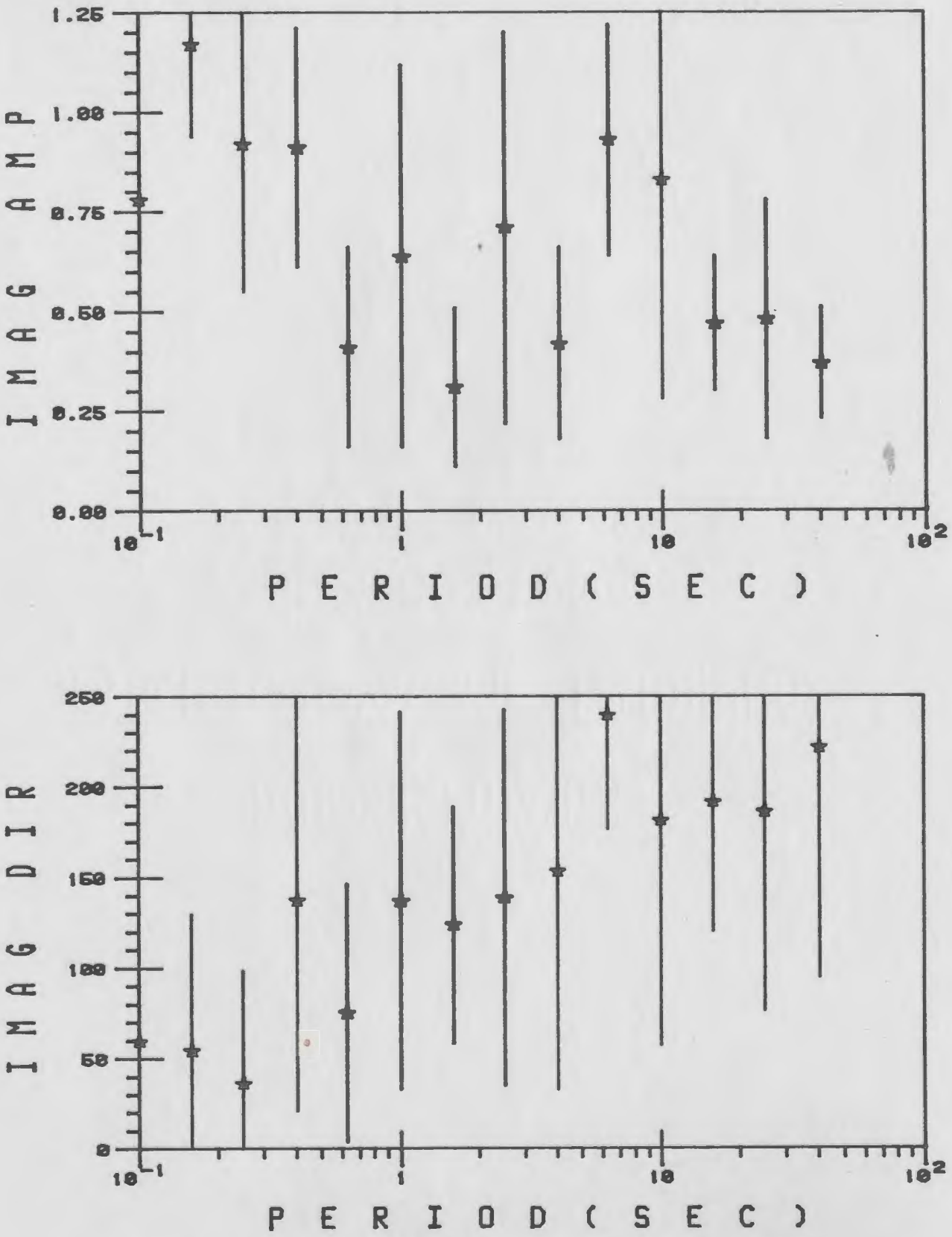

Fig. A9 Frequency and phase response of the imaginary (quadrature) arrows at BLR.

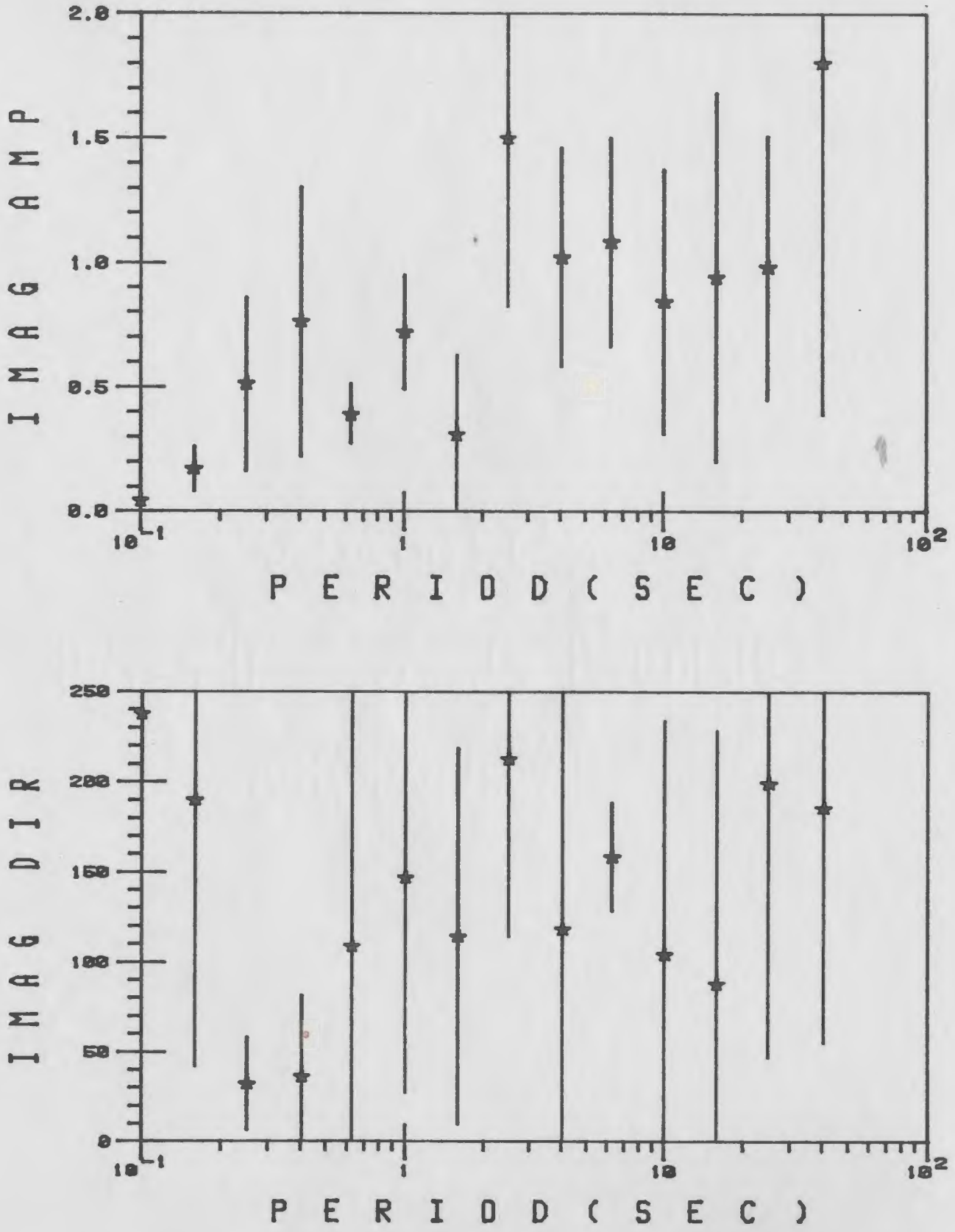

Fig. A10 Frequency and phase response of the imaginary (quadrature) arrows at GWD.

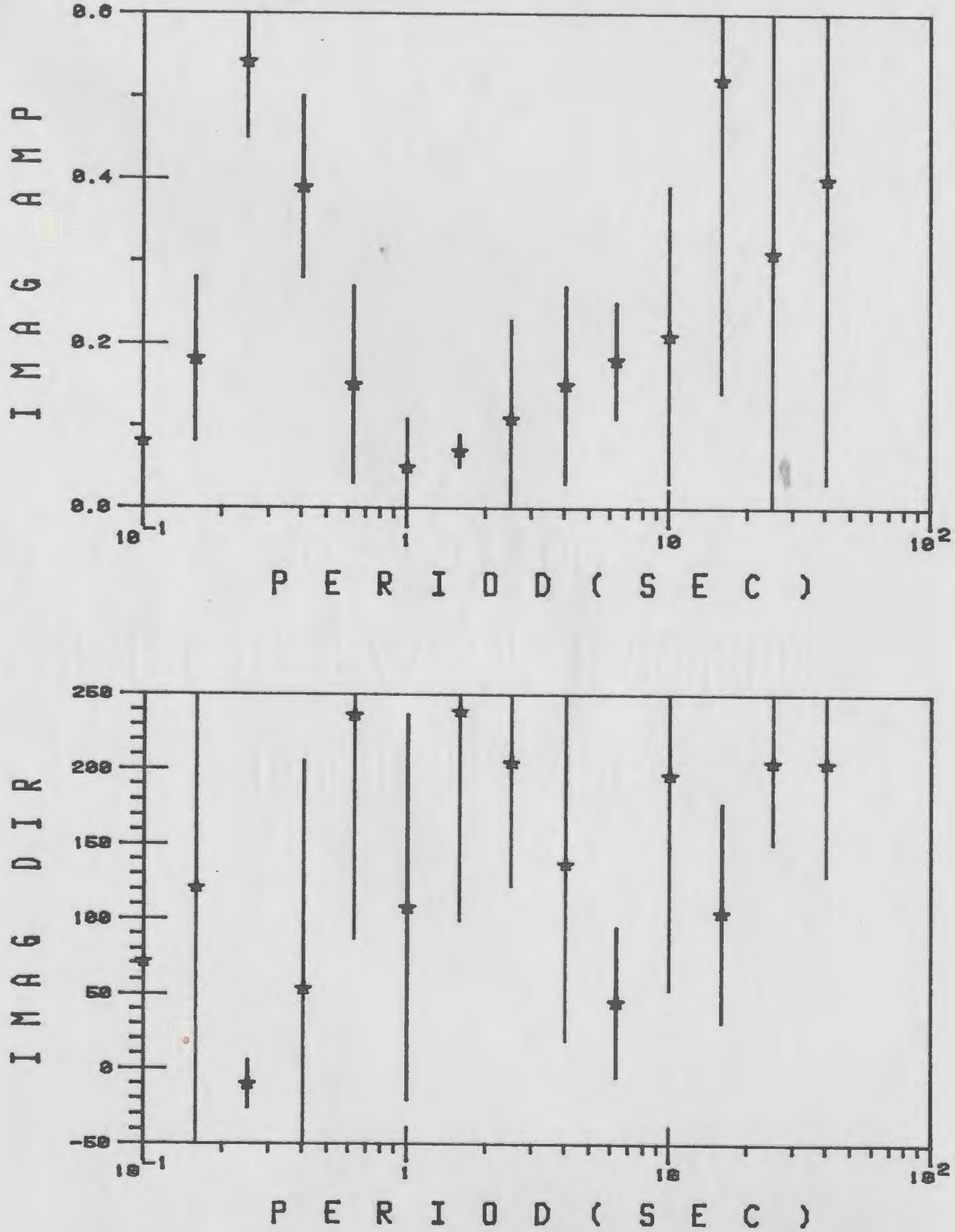

Fig. A11 Frequency and phase response of the imaginary (quadrature) arrows at JBR.

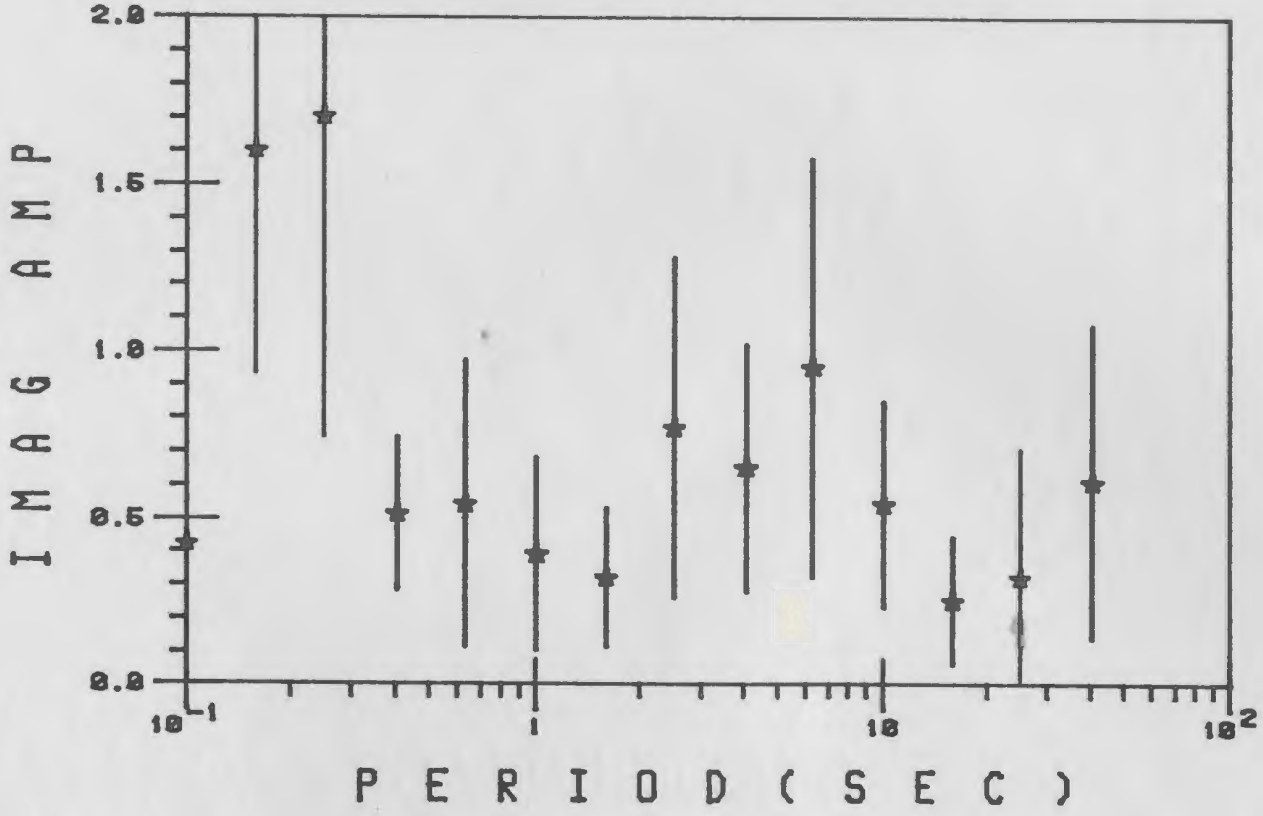

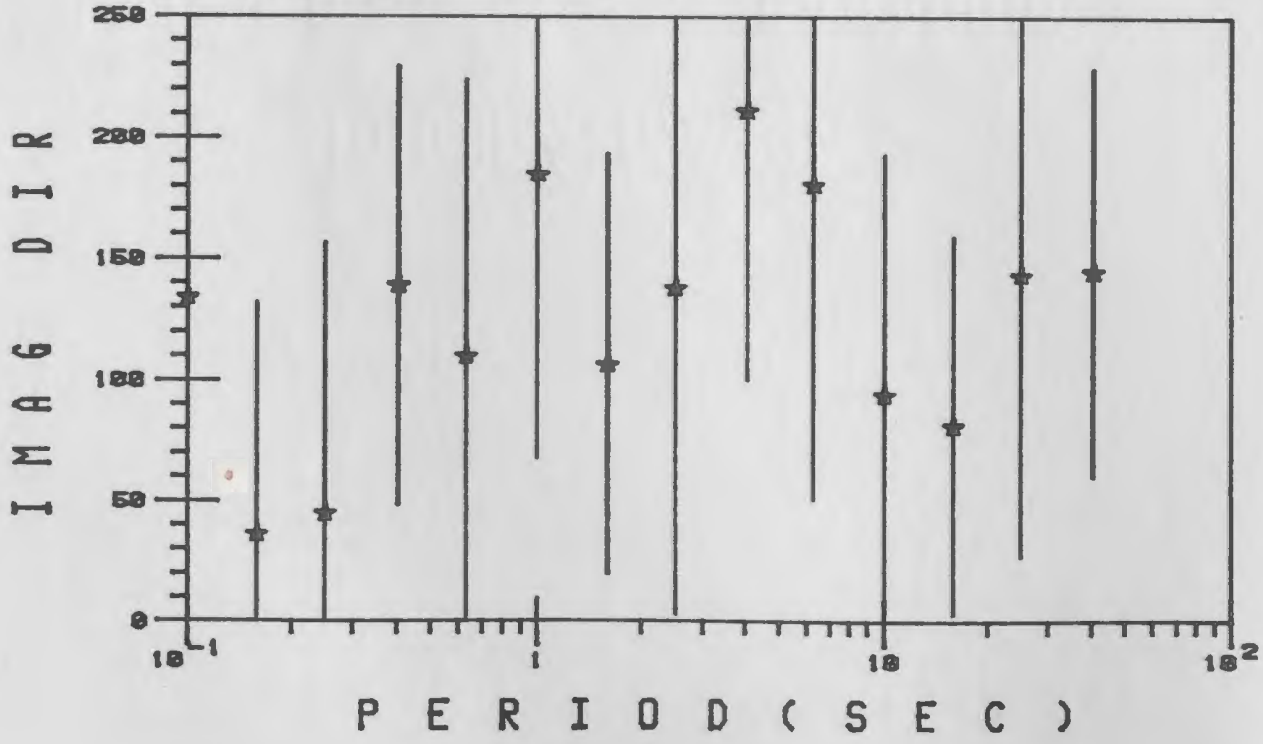

Fig. A12 Frequency and phase response of the imaginary (quadrature) arrows at GPR.

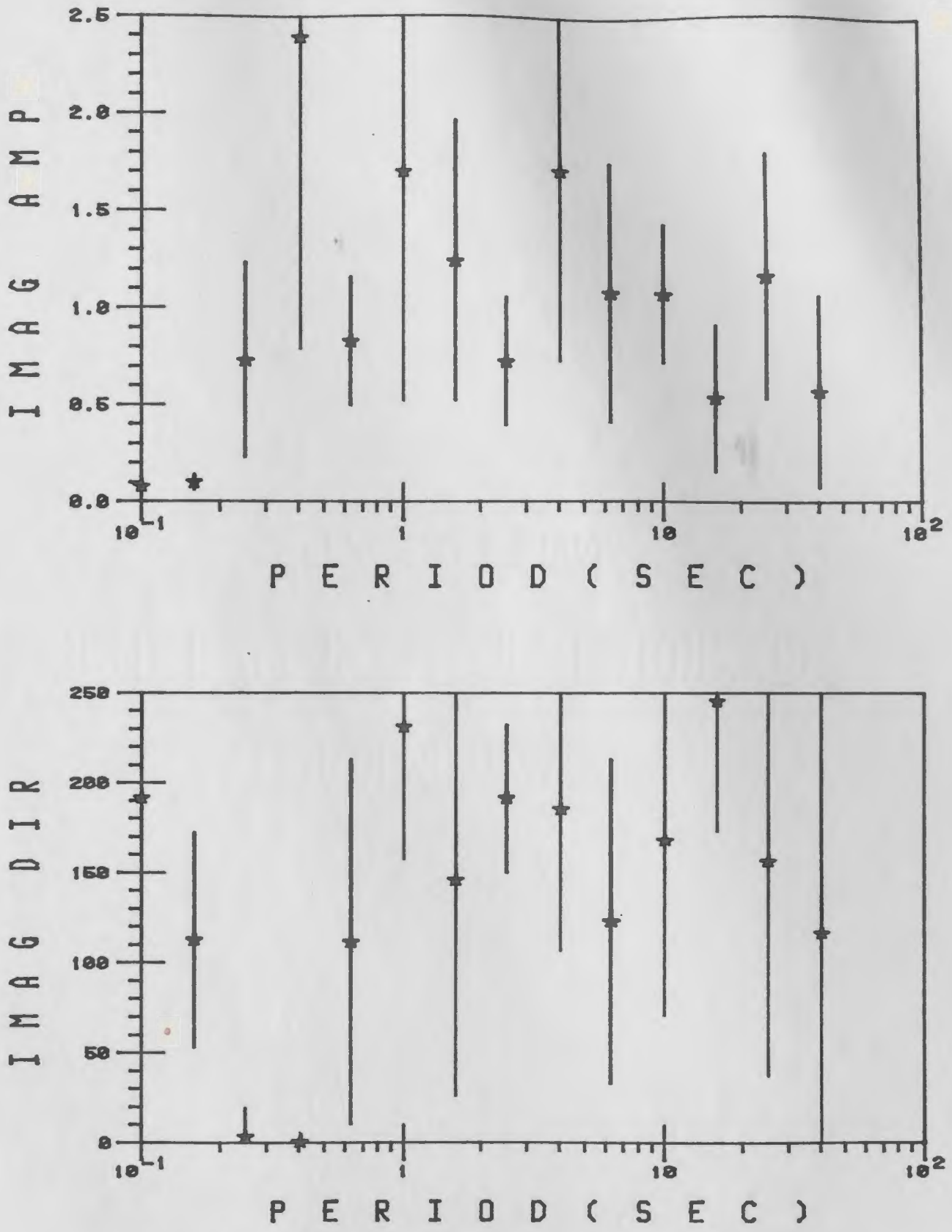

Fig. A13 Frequency and phase response of the imaginary (quadrature) arrows at TRN.

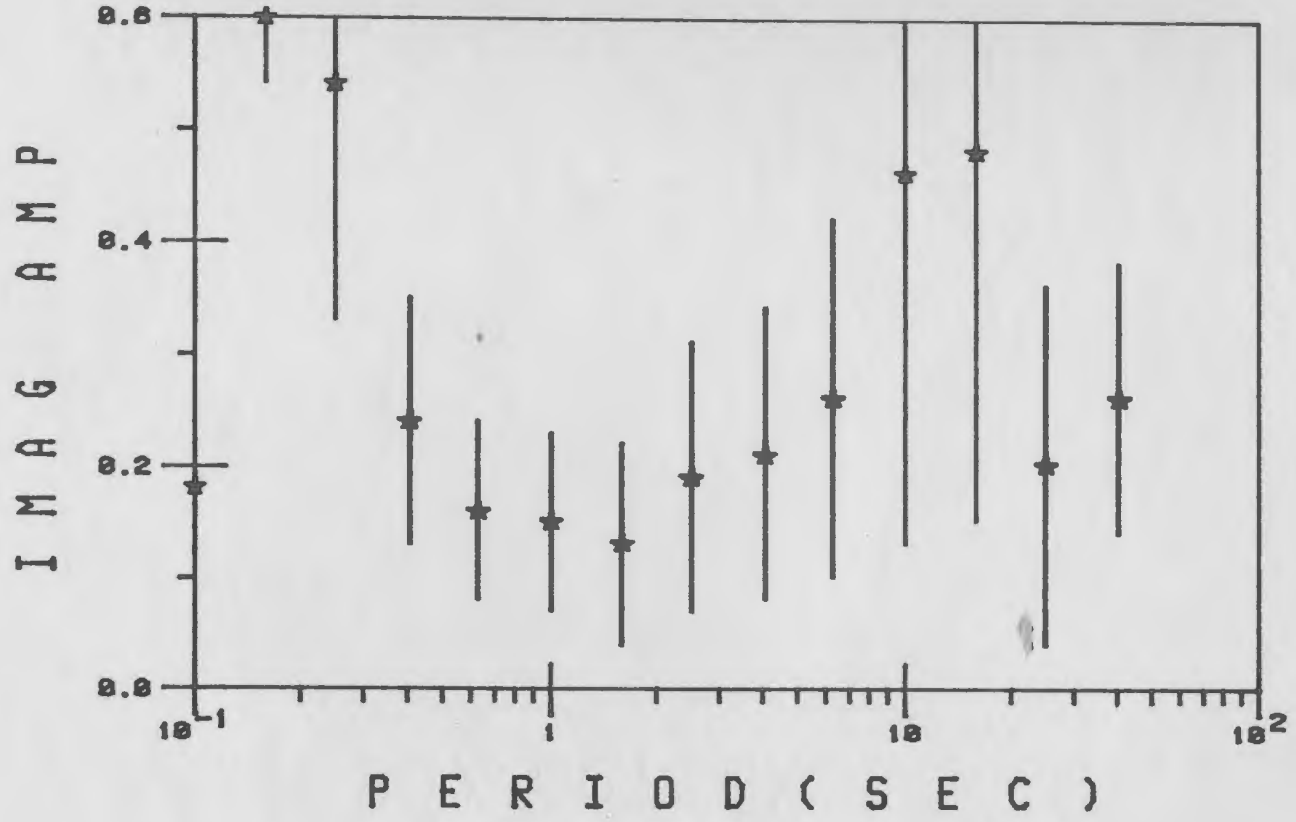

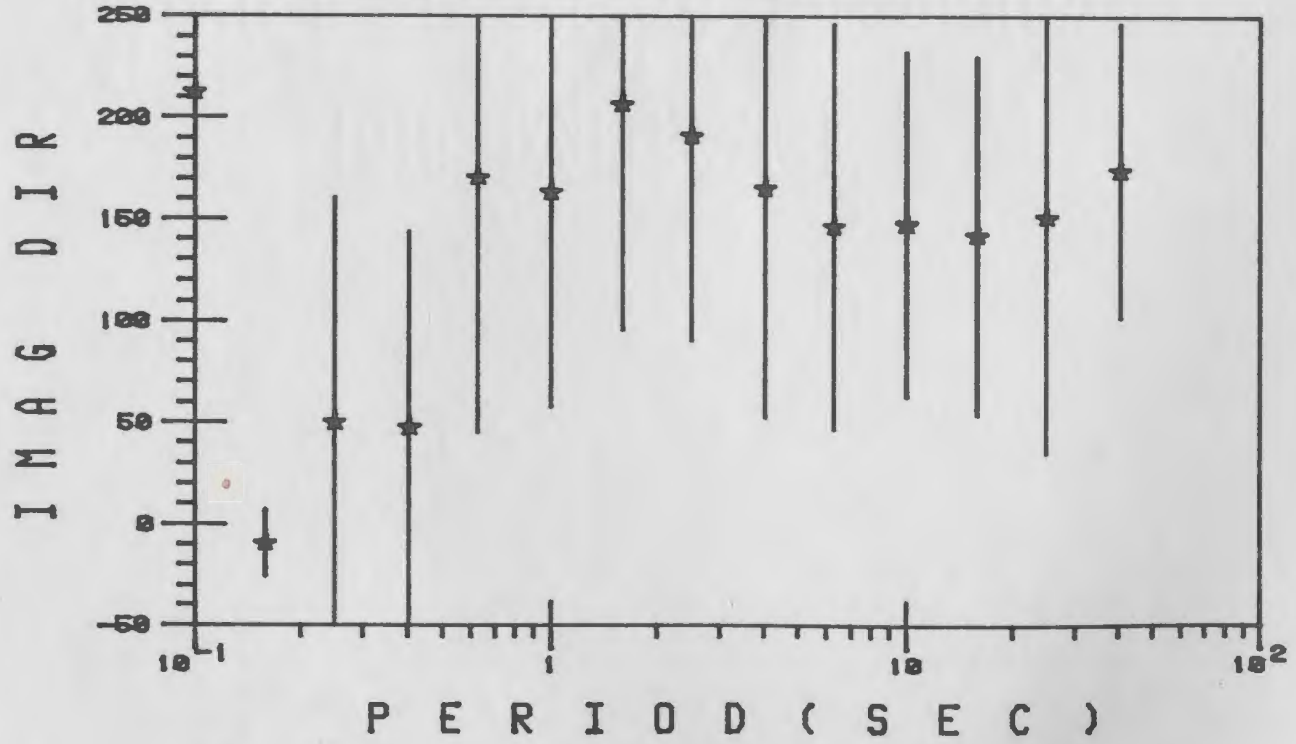

Fig. A14 Frequency and phase response of the imaginary (quadrature) arrows at CLV.

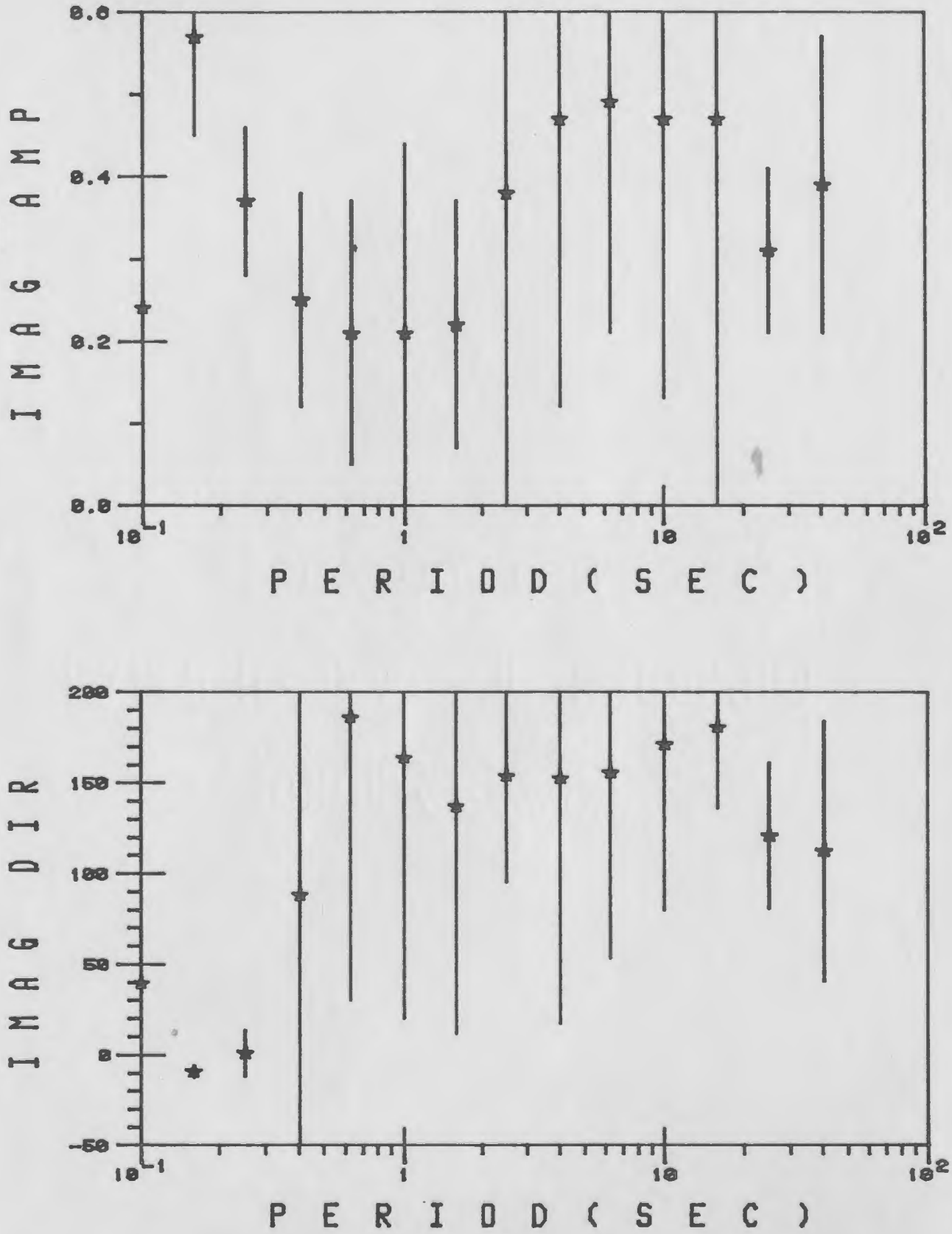

Fig. A15 Frequency and phase response of the imaginary (quadrature) arrows at GBS.

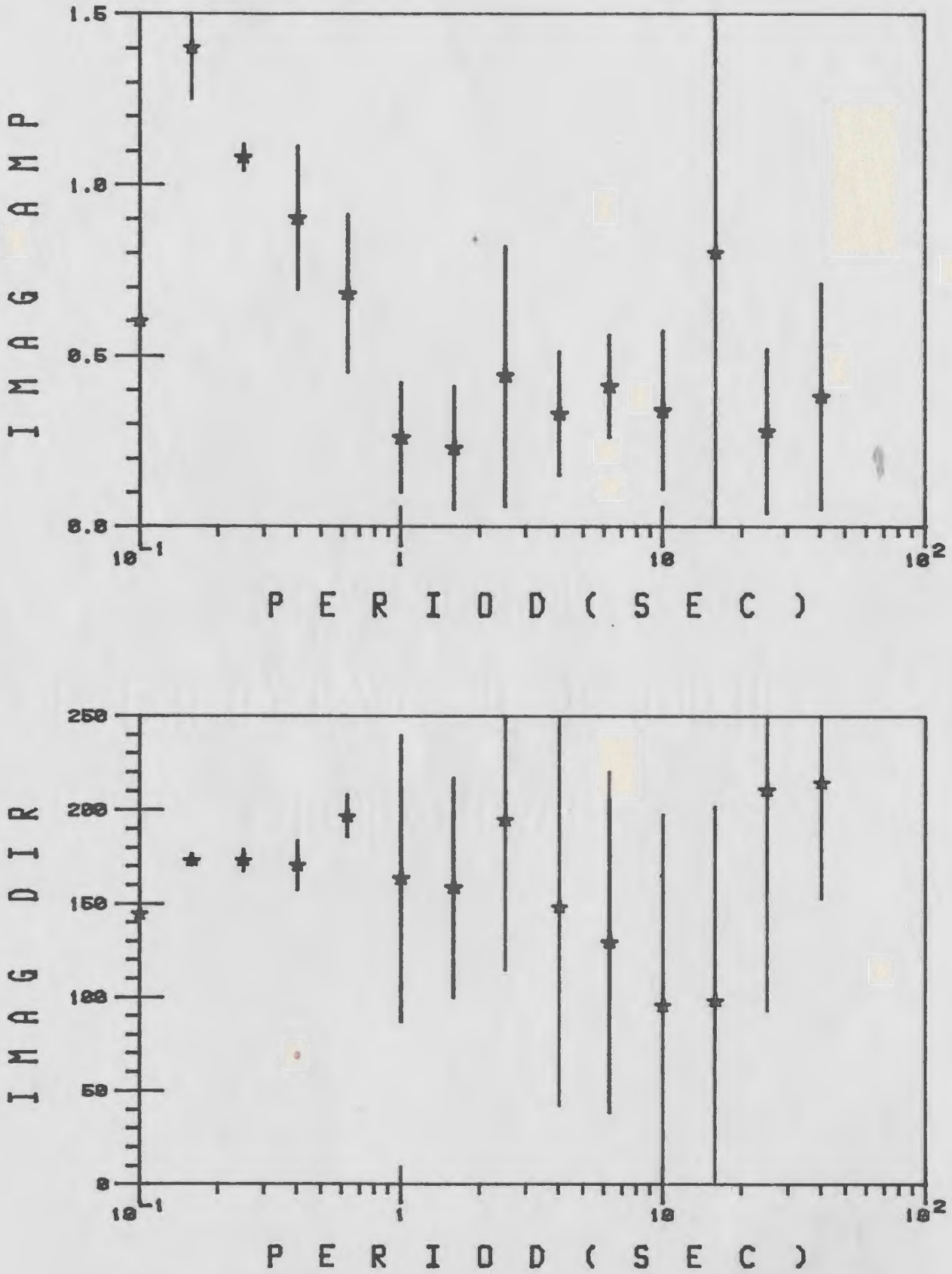

Fig. A16 Frequency and phase response of the imaginary (quadrature) arrows at WTB.